Typhoon Haiyan's sedimentary record in coastal environments of the Philippines and its palaeotempestological implications

Dominik Brill[1*], Simon Matthias May[1], Max Engel[1], Michelle Reyes[2], Anna Pint[1], Stephan Opitz[1], Manuel Dierick[3], Lia Anne Gonzalo[4], Sascha Esser[1], Helmut Brückner[1]

[1] Institute of Geography, Universität zu Köln, Germany
[2] Marine Science Institute, University of the Philippines, Philippines
[3] Department of Physics and Astronomy, Universiteit Gent, Belgium
[4] Nationwide Operational Assessment of Hazards (Project NOAH), Department of Science and Technology, Philippines

10   *Correspondence to:* Dominik Brill, Albertus-Magnus-Platz, 50923 Köln, Germany, brilld@uni-koeln.de

Abstract: On November 8th 2013, category 5 Supertyphoon Haiyan made landfall on the Philippines. During a post-typhoon survey in February 2014 Haiyan-related sand deposition and morphological changes were documented at four severely affected sites with different exposure to the typhoon track, and different geological and geomorphological settings. Extended onshore sand sheets are restricted to coastal areas with significant inundation due to amplification of surge levels in embayments or

15   due to accompanying long-wave phenomena at the most exposed coastlines of Leyte and Samar. However, localized washover fans with a storm-typical laminated stratigraphy occurred even along coasts with limited inundation due to waves overtopping or breaching coastal barriers. On a recent reef platform off Negros in the Visayan Sea, storm waves entrained coral rubble from the reef slope and formed a several 100 m long, intertidal coral ridge when breaking at the reef edge. As these sediments and landforms were generated by one of the strongest storms ever recorded, they not only provide a recent reference for

20   typhoon signatures that can be used for palaeotempestological and palaeotsunami studies in the region, but might also function as a benchmark example for a general discrimination between storm and tsunami deposits. Even for sites with low topography and high inundation levels during Supertyphoon Haiyan, the landward extent of the documented sand sheets seems significantly smaller than typical sand sheets of large tsunamis. This criterion may potentially be used to distinguish both types of events.

25   **Keywords:** typhoon; tropical cyclone; storm deposit; storm versus tsunami; sand sheet; washover fan; coral ridge; Philippines

1. Introduction

On November 8th 2013, Typhoon Haiyan (local name: Yolanda) made landfall on the Philippines reaching category 5 on the Saffir-Simpson Hurricane scale. By crossing the archipelago Haiyan caused more than 6000 casualties, affected more than 16 million people, and damaged more than 1 million houses (NDRRMC, 2014; Lagmay et al., 2015). Its destructive power resulted

30   from exceptional surface winds reaching sustained velocities of up to 315 km/h (1-minute averaged data), gusting even up to

380 km/h, in combination with massive storm surge flooding with water levels up to 9 m above tide level (IRIDeS, 2014). Based on recorded wind speeds and core pressure, Haiyan was not only an exceptional event for the Philippines but one of the most powerful tropical cyclones ever recorded. Against the background of the ongoing controversial discussion on the influence of climate change on cyclone frequencies and magnitudes (Knutson et al., 2010; Pun et al., 2013), Typhoon Haiyan

5   could be both an exceptional low-frequency event and/or a precursor of a new normality.

The need for robust data that provide information about long-term typhoon risk in affected areas is highlighted by the lack of awareness and preparedness of many inhabitants regarding Haiyan (Engel et al., 2014; Lagmay et al., 2015). Similar to other coastal disasters in the immediate past, such as the 2004 Indian Ocean Tsunami (Brückner and Brill, 2009) or Cyclone Nargis in 2008 (Fritz et al., 2009), studies of occurrence patterns and effects of past flooding events with exceptional magnitude have

10   been lacking in the Central Philippines. Although previous catastrophic typhoons with similar tracks have been historically documented, e.g. in 1897 or 1984 (PAGASA, 2014; Soria et al., 2015), their disastrous effects have not been taken into account properly. This was at least partly due to limited comprehension of the term "storm surge", which people mainly associated with the moderate flooding of typical typhoons in the area (Engel et al., 2014; Mas et al., 2015). This discrepancy between real risk and perceived risk results from an underrepresentation of local high category typhoons in instrumental and historical

15   records, since the magnitude-frequency relationship of cyclones usually follows inverse power law functions (Corral et al., 2010).

Geological imprints of cyclones may be used to enhance existing historical and instrumental records, as they potentially cover periods of several millennia and, thus, document even events of the highest magnitudes in statistically significant numbers (Hippensteel et al., 2013; May et al., 2013, 2015a). However, using geological archives to extend tropical cyclone histories

20   requires the identification of tropical cyclone traces as well as reliable dating of event layers. In particular the discrimination of similar depositional events such as tsunamis is challenging (Shanmugam, 2012). In this regard, modern event deposits offer the possibility to establish (locally valid) event-specific criteria that indicate prehistoric events in the geological record (Nanayama et al., 2000; Kortekaas and Dawson, 2007). Likewise, they may help to evaluate reliable age (Bishop et al., 2005; Brill et al., 2012) and magnitude (Brill et al., 2014) reconstructions of palaeoevents. Since sedimentary signatures of cyclones

25   natuaare particularly influenced by local factors (Schwartz, 1982; Matias et al., 2008), Haiyan's geological footprint will primarily be useful to establish criteria for inferring past typhoons from geological records found in the same areas. However, as one of the strongest storms ever recorded, Haiyan might have the potential to pose a benchmark example for establishing geological signatures that add to the discussion on discriminating between tsunamis and extreme cyclones in general.

While the role of exceptionally large boulders moved by Haiyan for the interpretation of geological storm records has already

30   been discussed by May et al. (2015b), we report on sandy sediment data from four different Haiyan-affected coastal areas, collected during a post-typhoon field survey on the Philippines in February 2014, i.e. three months after Haiyan made landfall. The investigated areas comprise different geologies with carbonate and volcanoclastic coasts, as well as different geomorphological settings including steep cliff platforms, low coastal plains and coral reefs. Haiyan's impact on heavily affected coastal areas was documented by recording onshore and intertidal sedimentation, coastal erosion and

geomorphological changes, as well as indicators for inundation, run-up, flow depth, and flow direction. Based on these data, sedimentary and geomorphological storm signatures typical for the study area are established. Likewise, the spatial variability of typhoon imprints due to site-specific characteristics such as the local topography, bathymetry, and geology, as well as the exposure to the typhoon track is documented. As a second step, the potential of these modern typhoon deposits is evaluated in

5 respect of possible implications for the identification of prehistoric cyclones in the geological record.

2. Study area

The Philippine archipelago is located in the western Pacific Ocean between 5° and 20° northern latitude. Field work was carried out in three different areas (Fig. 1): (i) at the east coast of Samar between Llorente and General MacArthur (Fig. 1b); (ii) at the northeastern coast of Leyte between Tacloban and Dulag (Fig. 1b); and (iii) on several islands northeast of Northern

10 Negros (Sagay) including Bantayan (Fig. 1c). All three study areas were significantly affected by Typhoon Haiyan, but are characterized by a different exposure to the typhoon track and by particular geomorphological and geological settings.

2.1 Climate and typhoon activity

2.1.1 General climatic and hydrodynamic conditions

The Philippine islands are characterized by a subtropical climate influenced by monsoon winds and the ENSO system. While

15 the west of the archipelago experiences seasonal variations in rainfall and temperature with a dry period from November to April and a wet season during summer monsoon, the significance of seasonality gradually decreases towards the east reaching all-season wet conditions along the eastern coast (PAGASA, 2011). Hence, the study areas on Leyte and Samar show no pronounced annual rainfall variations. Northern Negros and Bantayan are influenced by weak monsoon seasonality. The highest swell waves occur during the winter monsoon and along the Pacific coast, while wave action during the summer

20 monsoon and within the Sea of Visayas is generally moderate (Fig. 1e, Navy METOC, 2014). Tidal variations are in the range of 0.8–1.8 m. In addition, the entire Philippine territory is located in the corridor of east-west moving typhoons. On average, 21 tropical cyclones hit the Philippines annually, whereas the occurrence probability increases markedly towards the north (Fig. 1d, PAGASA, 2014).

2.1.2 Haiyan's path over the Philippines

25 Starting as a tropical depression on November 3rd 2013 over the northwestern Pacific, Haiyan continuously gained intensity, turning into a tropical storm on November 4th, and a typhoon on November 5th. On November 6th Haiyan reached category 5 on the Saffir-Simpson Hurricane scale and finally made landfall on Samar on November 8th (IRIDeS, 2014). After its first landfall near Guiuan (Eastern Samar) at 4:40 am, Haiyan crossed the archipelago in a western direction without reducing its strength below category 5 (Fig. 1a). On its path over the Philippines, Haiyan made landfall on northern Leyte at 7:00 am, on

30 northern Cebu at 10:00 am, on Bantayan at 10:40 am, and later on Panay and Palawan (NDRRMC, 2014).

Depending on the exposure to the typhoon track, wind speeds, storm surge levels and wave heights varied significantly between the study sites. Additional variations are determined by differences in local bathymetry, fetch and shape of the coastline (see section 2.2). In general, coastal flooding rapidly reached peak levels that lasted for approximately two hours and was characterized by multiple pulses of inflowing waves with periods of several seconds (Mas et al., 2015; Morgerman, 2014).

5 However, south of Tacloban, up to three distinct flooding pulses approached in periods of a few minutes (Mas et al., 2015), and along the coast of Eastern Samar surprisingly high values of run-up and flow depth were documented (Tajima et al., 2014; May et al., 2015b). While successive flooding pulses may be explained by seiches in semi-enclosed basins such as the San Pedro Bay (Mori et al., 2014), the inundation pattern along the open coast of Eastern Samar may suggest additional overprinting of storm waves through surf beat (Bricker et al., 2014).

10 (i) The exposed coast of Eastern Samar is characterized by a large fetch and a steep offshore bathymetry. Hence, it experienced maximum wind speeds with the highest model-predicted waves of up to 20 m, but only a limited wind-driven surge (Bricker et al., 2014). Field evidence documents flooding levels of up to 6 m onshore flow depth, nearly 11 m run-up above storm tide (a.t.l.), and up to 800 m inundation distance (PAGASA, 2014; Tajima et al., 2014; May et al., 2015b). (ii) The northeastern coast of Leyte was still exposed to the full strength of the storm winds, since the landmasses to the east are too narrow to

15 significantly reduce Haiyan's intensity. However, due to the shallow water and the resonance effects in the enclosed embayment (Mori et al., 2014), storm-water levels were dominated by a surge setup, while model-predicted wave heights were <5 m (Bricker et al., 2014). Field evidence shows that the storm surge reached flow depths of 6 m, run-up levels of nearly 8 m a.t.l., and inundation of several hundred meters inland (Mas et al., 2015, Tajima et al., 2014). (iii) Smaller surge levels and moderate wave heights were modelled for Northern Negros and Bantayan (Bricker et al., 2014), due to a shallow bathymetry,

20 low tide at the time of landfall and the sheltering landmasses of Samar, Leyte and Cebu to the east. Likewise, eyewitness accounts document maximum onshore flooding levels of only 1.50 m a.t.l. (Cuadra et al., 2014).

2.2 Geology and geomorphology

The Philippine islands are formed by a complex geological structure of north-south running volcanic arcs, tectonic basins and fragments of continental crust reflecting subduction and collision processes between the Eurasian and the Philippine plates.

25 As the main tectonic structures, the Philippine and Manila trenches confine offshore subduction zones to the east and west of the archipelago, while the Philippine Fault crosses the archipelago in an axial position from north to south (Fig. 1a, Rangin et al., 1989). The associated volcanoes and ophiolites form islands dominated by steep, cliff-lined coasts that are bounded by fringing reefs and are occasionally intersected by flat alluvial lowlands and pocket beaches. The clastic beaches are characterized by either white sand originating from coral reefs, or darker minerals derived from volcanic provinces (Bird,

30 2010).

(i) The rocky carbonate coast of Eastern Samar typically shows steep headlands with cliffs formed of Pleistocene coral limestone and occasional pocket beaches bordered by fringing reefs (HER, Fig. 1b). Since the shelf bordering the Philippine

Trench is narrow (the 200 m isobath is <3 km offshore) and the fetch over the Pacific is not restricted, Eastern Samar is exposed to high swell waves especially during the winter monsoon (Fig. 1e) (Bird, 2010). (ii) Although Leyte is formed by ophiolitic and volcanic rocks as well, its northeastern coast is dominated by alluvial plains, sandy beaches and beach-ridge plains (TOL, Fig. 1b, Dimalanta et al., 2006). Rocky promontories and fringing coral reefs are scarce. Water depths in the shallow, funnel-shaped San Pedro Bay between Leyte and Samar do not exceed 30 m (Bird, 2010). (iii) In contrast to its mountainous interior dominated by volcanic rocks, the northeastern coast of Negros is characterized by wide coastal plains bordered by mangroves and extensive coral reefs (Rangin et al., 1989). Within the shallow water of the Visayan Sea to the north (water depths mainly <50 m) numerous coral islands occur (CAR and MOL, Fig. 1c). The island of Bantayan represents the northeastern limit of the coral islands. The raised limestone formations making up the island are completely surrounded by fringing reefs that partly border steep rocky coastlines, but are also associated with sandy beaches (BAN A and B in Fig. 1c, Bird, 2010).

3. Methods

The topography of all studied locations was documented along shore-perpendicular transects by means of a Topcon HiPer Pro differential global positioning system (DGPS) at 14 Feb at ~4 pm (TOL), 17 Feb at ~4 pm (HER), 23 Feb at ~10 am (BAN A), and 23 Feb at ~3 pm (BAN B). To reconstruct flooding characteristics of Haiyan's storm surge, indicators for onshore flow depth and run-up height were recorded by levelling debris lines, grass or floated debris in trees and bushes, as well as impact marks in the bark of palm trees relative to the sea level (all altitudes given in meters above Philippine height datum, a.s.l.). Onshore flow directions were deduced from oriented grass and trunks using a compass. In addition, comparison of rectified pre- and post-Haiyan satellite images was used to estimate inundation areas. Sediments and depositional landforms generated by Typhoon Haiyan were documented both onshore and in the intertidal zone. This included sandy deposits as well as coral-rubble ridges. Shore-perpendicular trenches were used to describe and document the stratigraphy of sandy deposits directly in the field. For detailed sedimentary and faunal analyses, sediment from Haiyan's deposits and reference environments was taken in the form of bulk samples from each stratigraphical unit at different distances from the shoreline, as well as push cores from at least one representative storm deposit at each investigated location.

To deduce transport processes, mode of deposition, and source environments of the storm deposits, we analysed fine-grained samples in terms of their granulometry, geochemistry, mineralogy and faunal composition at the Institute of Geography, University of Cologne. Grain-size analyses were performed with a Laser Particle Analyser (Beckman Coulter LS 13320) for material <2 mm after pre-treatment with H_2O_2 and $Na_4P_2O_7$ to remove organic carbon and to avoid aggregation. In case of samples with grain size >2 mm, the granulometry was determined on dried sediment using a Camsizer (Retsch Technology). Statistical parameters (mean, sorting, skewness) of grain-size distributions were calculated with the GRADISTAT software (Blott and Pye, 2001) using the formulas of Folk and Ward (1957). Further information about flow directions and mode of deposition was obtained by visually interpreting sedimentary structures in µCT scans with 50 µm voxel resolution (using myVGL 2.1 software) performed on two selected push cores (BAN 4 and TOL 8) at the University of Ghent, Belgium.

The chemical characterization of deposits includes determination of organic carbon by means of loss on ignition (LOI) measured after oven-drying at 105 °C for 12 h and ignition in a muffle furnace at 450 °C for 4 h. Carbonate contents were measured gas-volumetrically using the Scheibler method. The bulk-mineralogical composition was determined by X-ray diffractometry (XRD) on powder compounds performed on a Siemens D5000 using a step interval of 0.05° and a dwell time of 4 seconds. A fixed 1° divergence and antiscatter slit was used at diffraction angles from 5 to 75° 2theta. The Cu K-alpha radiation source was operated at 40 keV and 40 mA. The data were analysed with DiffracPlus Eva software package (Bruker AXS, Berlin, Germany).

Magnetic susceptibility (MS) was measured with a Geotec MSCL core sampler. For microfaunal analyses, samples were sieved to isolate fractions >100 and <100 µm. At least 100 foraminifers were identified to species level, if possible, and counted under a binocular microscope. States of reworking were assessed semi-quantitatively on the basis of test taphonomy and classified as no, low, medium, or strong reworking. To select appropriate parameters for interpreting transport processes and sediment source areas, we carried out principal component analysis (PCA) using PAST software (Hammer et al., 2001) after removing foraminifera species with insignificant abundance (i.e. <5 individuals in all samples) and correlating parameters based on Spearman's rank correlation coefficient (≥0.95).

4. Results – Sedimentary and geomorphological structures

4.1 Eastern Samar – Hernani (HER)

At barangay Batang, municipality of Hernani (HER, Fig. 1b) the Pleistocene reef retreats to a position more than 300 m from the shoreline, resulting in a gently inclined sandy coast (Fig. 2). For Haiyan, local residents report complete inundation of the lower coastal plain with water levels of several meters a.s.l., while Agaton and Basyang – the two tropical storms/depressions recorded between Haiyan and this field survey on January 19th and February 1st respectively (Fig. S3) – caused no significant flooding (Tab. S1 in online supplement).

Starting at the shoreline behind a 550 m wide intertidal reef lagoon and destroyed mangrove stands, the shore-perpendicular transect crosses a sandy beach ridge with a crest height of 3 m a.s.l. at 70 m from the shoreline. Landwards, the tree-covered back-barrier depression is crossed by a shore-parallel channel before shallow reef outcrops occur at 180 m transect length. After a second depression cultivated with rice fields (200–250 m), the transect ends at the inactive cliff of the elevated Pleistocene reef platform at 260 m inland and 3.6 m a.s.l. While swash lines document maximum inundation that exceeded the inactive cliff, floated grass and litter in trees indicate flow depths of at least 3.2 m a.s.l. or 1.5 m above surface (a.s.) at 150 m, up to 5.7 m a.s.l. (3.7 m a.s.) at 200 m, and heights of 3.7 m a.s.l. (1.4 m a.s.) at 260 m (Fig. 2).

Erosion was the dominant process seaward of the beach ridge, which is marked by an erosive scarp. Behind the barrier, sedimentation of sand and coral rubble was documented (HER 3–10), reaching its landward limit at the foot of the inactive cliff. A sharp contact separates the light brown sandy layer covering the dark brown, densely rooted pre-Haiyan soil (Figs 4b,

c). The thickness of the deposit decreases rapidly landwards, from 20 cm directly behind the beach ridge (HER 9) to only 2 cm at 150 m (HER 7) and a few mm at 260 m (HER 3). Coarse coral clasts at the surface (up to ~20 cm) occur as far as 100 m inland. Along the same section, a fining trend from a modal grain size of 1.3 cm to 223 µm is observed (Figs 3, 4a).

Two different sedimentary facies units can be distinguished: Unit 1 was not encountered in HER 9 but comprises the entire typhoon deposit in HER 3–8 and 10 (Figs. 4a, b). It is characterized by massive (HER 3-7) or slightly laminated (HER 8, 10), poorly sorted (3.4-7.3) fine-medium sand (mean of 85-570 µm) and is thinning and fining landward from 8 cm and a mean of 570 µm at 130 m from the shoreline (HER 8) to only 3 mm and a mean of 223 µm at 260 m (HER 3) (Fig. 3). Unit 2 is significantly coarser than unit 1 (modes at 1.2 mm and 2.7 cm) and is only present at HER 9 (Fig. 4c). At HER 9 it forms a 15 cm thick layer with steeply landward inclined layering and numerous angular coral fragments (constituting 77% of total mass). Both units are dominated by carbonates (nearly 100% Mg-calcite and aragonite). The foraminifera assemblage (determined for HER 10) is dominated by *Calcarina* sp. (41%), *Amphistegina* sp. (21%) and *Baculogypsina sphaerulata* (12%) that show significant reworking (<8% fresh tests, >50% strongly reworked). Vertical variations of species composition and taphonomy within HER 10 roughly correlate with changes in grain size (Fig. 4d).

4.2 Northeast Leyte (Tolosa)

Flood levels in Tacloban and in the coastal barangays to the south (Fig. 1b) reached >6 m a.s.l. and locally, inundation extended up to 1 km inland (Tajima et al. 2014). The typhoon was accompanied by strong wind damage with uprooted trees, heavy beach erosion and onshore sedimentation. Due to the position to the typhoon centre – winds and surge are strongest to the right of the typhoon track – water levels, beach erosion and sedimentation continuously decreased towards the south.

Although – according to surge levels – thickest onshore deposits are to be expected in Tacloban and directly south of it, we report on the storm impact on the nearshore area of Tolosa's beach-ridge plain (TOL, Fig. 1b), since the northern areas are more densely populated and unaltered typhoon sediments were hard to find three months after Haiyan. According to floated grass found in trees and bushes, Haiyan overtopped the 2.5 m high beach ridge and inundated the marshy back-barrier depression with flow depths of at least 5 m a.s.l. (3.5 m a.s.) at a distance of 70 m from the shoreline (Fig. 5). At the landward end of the transect, 300 m from the shoreline, water levels of at least 3.5 m a.s.l. (1.8 m a.s.) have been recorded and satellite images for the Tolosa area document a landward flooding extent of up to 800 m during Haiyan (Fig. 5a). However, since sandy deposition stopped even more seaward, any further documentation was beyond the scope of this survey. The direction of onshore flooding is indicated by grass bent down in a NW-NNW direction, a westward collapsed north-south running wall structure, and the NW orientation of floated palm trunks (Figs 5b, c).

An erosive scarp at the seaward slope of the beach ridge indicates coastal erosion by Typhoon Haiyan that had already partially recovered in February 2014. Pre and post-typhoon satellite images show a shoreline retreat of 25–30 m (inset in Fig. 5b). Between 30 and 250 m inland, a sheet of dark grey sand was deposited (TOL 3–14, Fig. 6). While 5–10 cm of sediment were accumulated on top of the beach ridge (TOL 3–4), the maximum thickness of 10–20 cm is reached directly leeward of the

barrier (TOL 5–8). Further landward, the thickness rapidly declines, reaching 2–5 cm at 70–90 m from the shoreline (TOL 9–11) and only a few millimetres landwards of TOL 11 (TOL 12–14).

Investigations of profiles TOL 5 and 7 reveal the complete absence of carbonate components and microfauna in the storm layer. Instead, the composition is dominated by a mixture of feldspar (30–70%), amphibole (20–40%) and a minor percentage of quartz (5–30%). Magnetic susceptibility and LOI help to discriminate typhoon deposits from the underlying soil, but have constant values within the storm layer (Fig. 6c). However, in the stratigraphy of TOL 7 (Fig. 6b) and in the μCT scan of TOL 8 (Fig. 7), a normally graded unit 1 with scour marks at the base is clearly discriminated from the successive horizontally laminated unit 2 within the Haiyan deposits.

Unit 1 forms a layer of fine to medium sand at the base of profiles TOL 7–14. It covers the pre-Haiyan soil and, at several places, bended stems of grass. In profiles TOL 9–14, unit 1 constitutes the entire event deposit and is covered by a thin mud cap (Fig. 6a). While it is well-sorted (1.5–1.7) throughout the entire transect, its thickness decreases in a landward direction from 3–5 cm behind the beach ridge (TOL 7–10) to <1 cm at TOL 11–14. A landward fining trend has been noted as well (Fig. 3). Unit 2 comprises a well-laminated layer of mainly medium sand (Figs 6, 7) and makes up the upper part of the storm layer in the proximal part of the transect (TOL 3–8). The lamination is due to alternating concentrations of pyroxene (dark) and quartz (light) (XRD results, Fig. 8a). In TOL 5, the laminae are slightly inclined landwards and show repeated coarsening and fining sequences (Fig. 6c). Unit 2 forms a washover fan at the landward slope of the beach ridge. While no clear trend in the thickness of the deposit was found – values range between 5 cm at the top of the beach ridge (TOL 4) and the landward edge of unit 2 (TOL 8), and ~20 cm directly behind the ridge (TOL 5) – it slightly thins landward (Fig. 3). Sorting is similar to unit 1 (1.5–1.6), but the mean grain size (245–328 μm) is slightly coarser.

4.3 Northern Negros

All visited coral islands north of Negros (Carbin, Molocaboc, Suyac, Fig. 1c) were affected by moderate flooding with changing wind and wave directions from NNE before to WSW after the passage of Typhoon Haiyan's centre (Tab. S1, online supplement). Substantial beach erosion associated with onshore transport of sediment was observed directly after Haiyan. While coral rubble ridges were formed in the intertidal zone of Suyac and Carbin (CAR), onshore deposition was restricted to thin sand patches and small coral boulders or parts of sea walls (main axis <2 m) in the proximal coastal zones of Molocaboc (MOL) and Suyac.

4.3.1 Carbin Reef (CAR)

On Carbin Reef, a coral rubble ridge along the western edge of the reef platform is visible at low tide (Fig. 9), but entirely submerged at high water. According to local fishermen, the ridge did not exist in its present form prior to Haiyan (Tab. S1, online supplement), which means that it had either been absent or significantly lower (Reyes et al., 2015). The average crest height of the more than 300 m long section of the ridge measured during the field survey is 0.55 m a.s.l. (0.45 m above mean

low water, single boulders reach heights of 1.20 m a.s.l.) without a significant trend in either direction. The basal width is 10–20 m, and lobe structures at its landward side cover corals in living position that must have been alive prior to the typhoon. Morphology and sediment – the ridge is mainly composed of centimetre to decimetre large coral fragments – allows the discrimination of two units: lobes of greyish, algae-covered coral rubble extending up to 20 m landward (unit 1), and light,

5   freshly broken coral branches that form steep lobes or patchy coverings extending no more than 10 m from the reef edge, on top (unit 2). While both units are present along the entire 300 m long section, they significantly broaden from 10 m to 20 m width along the northern section (Fig. 9).

4.3.2 Molocaboc Island (MOL)

At Molocaboc (Fig. 10), the coastal zone behind the 550 m wide intertidal platform of the fringing reef is formed by a beach
10   ridge with a crest height of 3.1 m a.s.l., followed by a shallow back-barrier depression densely covered by acacia shrubs at 2.70 m a.s.l. Behind the beach ridge, fresh sandy deposits that rapidly thin landwards from 10 cm at 20 m shoreline distance to only 1 cm at a distance of 45 m have been recorded. The medium to coarse (mean = 600–680 µm), moderately sorted (1.7–1.8) sand shows no apparent sedimentary structures and a calcareous composition (>90% Mg-calcite and aragonite); the Foraminifera assemblage is dominated by *Calcarina* sp. (58%) and strongly reworked tests (<18% fresh). The storm deposit
15   contrasts with the underlying soil which is poorly sorted (3.4–4.7) and shows elevated contents of organic matter (4–7%) and reduced carbonate concentrations (70–80%). A reference sample from the subtidal zone (R_{subt}) is slightly finer (mean = 310 µm), moderately sorted (2.4), and dominated by different foraminifera (*Quinqueloculina* spp. [18%], *Peneroplis pertusas* [17%], *Elphidium* sp. [14%], *Ammonia beccarii* [12%]) with moderate reworking (74% fresh).

4.4 Bantayan

20   Eyewitnesses report limited storm surge elevations with moderate waves and peak flooding arriving at low tide for the entire east coast of Bantayan (Tab. S1, online supplement). However, while onshore deposition is restricted to sand sheets of a few centimetres in coastal areas directly behind active beach ridges, beach erosion of several meters did occur. More pronounced flooding happened only locally at the mouths of estuaries and resulted in the formation of small washover fans (BAN A and B, Fig. 1c).

25   ### 4.4.1 Bantayan A (BAN A)

At BAN A, the NE-exposed beach section (Figs 11a, b) is separated from an estuary river mouth by outcrops of the Pleistocene coral reef limestone with 1–2 m high cliffs. Cross sections reveal a succession of shore-parallel beach ridges with elevations of 2.1–2.3 m a.s.l. that are interrupted by ~1 m deep swales (Fig. 12a). While recent flooding levels were indicated by debris lines at 2 m a.s.l. along the seaward and landward slopes of the second beach ridge, as well as on top of the 3.5 m high reef
30   platform to the NW, the maximum wave height during Haiyan was estimated to have reached 3.6–4.0 m a.s.l. on the basis of eyewitness accounts (Tab. S1, online supplement). Furthermore, residents report flooding of approximately 50 m inland and

strong beach erosion during Haiyan. However, for this section of the coast (E1–E5, Fig. 1c) similar effects were observed after tropical storm Basyang in February 2014 which had been less intense, but had struck at high tide (Fig. S3 and Tab. S1, online supplement).

Storm erosion created a steep shoreface with an erosive scarp and uprooted palm trunks at the seaward slope of the first beach ridge. Residents report lateral erosion of more than 5 m due to the combined influence of Haiyan and Basyang along large sections of the beach (Tab. S1, online supplement). However, the formation of lobate washover fans in the back-barrier depression is already visible on satellite images from November 2013 (Fig. 11b). The washover fans are restricted to a 10 m wide section behind the beach, but form prominent landforms with two distinct stratigraphical units (Figs 11c, 12a).

The basal unit 1 is related to flat washover lobes characterized by planar lamination. It overlies a weakly developed soil with a sharp contact and extends slightly further inland compared to the subsequent unit 2, which is characterized by landwards inclined beds with a steep terminal front. The internal structure is illustrated by the sedimentology (Fig. 12b) and µCT scans (Fig. 7) of sediment core BAN 4. Below the pre-Haiyan soil, a thin sheet of medium sand (PE) was found along the erosive cliff in the ridge (Fig. 12a) as well as in BAN 4 (Figs. 7, 12b). The sand layer covers an older palaeosol, composed of brown, slightly loamy sand. The basal Haiyan deposit is composed of a laminated section of medium-coarse sand (mean of 600-770 µm), rich in strongly reworked foraminifer tests (35-60%) dominated by *Calcarina* sp. and *Amphistegina* sp. (unit 1). The uppermost 19 cm (unit 2) are composed of coarser sand (mean of 730-1300 µm) with similar species composition but a higher percentage of fresh or only slightly reworked foraminifers (60-80%) between 19 and 10 cm b.s. (Fig. 12b).

4.4.2 Bantayan B (BAN B)

Site BAN B is located in direct vicinity of an estuary mouth in northern Bantayan, lined by a 500 m wide intertidal reef platform (Fig. 11d). While the coast south of the estuary is characterized by a 3.4 m high cliff in the Pleistocene coral reef limestone, a c. 100 m wide sand spit backed by mangroves forms the section to the north (Fig. 11e). In a shore-perpendicular direction, a 3 m high beach ridge is followed by a flat mud plain with mangroves and reef outcrops at 1.5–1.7 m a.s.l. (Figs. 13a, S1). Eyewitnesses report significant flooding by Typhoon Haiyan, while Basyang – different from the southern part of Bantayan – caused no marked inundation (E6–10 in Tab. S1, online supplement). Flood marks in the form of floated debris on top of the cliff or trapped in bushes and mangroves document inundation of at least 200 m inland. Minimum flow depths decrease landwards from 3.7 m a.s.l. directly at the coastline, to 2.7–2.9 m a.s.l. at 60 m from the shoreline and only 2 m a.s.l. at 160 m (Fig. 11e).

Haiyan-induced onshore sand deposition is less than 1–2 cm in the back-barrier mangroves. Thicker deposits occur in the form of up to 30 cm thick and 50 m wide washover fans at two sections behind breaches in the barrier (Fig. 11e). Coast-perpendicular transects (T2 and T3, Fig. 11e) reveal landward thinning trends from 28 cm at 10 m behind the barrier to only 5 cm at a distance of 40 m (T2, Fig. 3), and from 15 cm at 10 m behind the ridge to 1 cm at a distance of 40 m respectively (T3 in Fig. S1a, online supplement). Similar to site BAN A, the pre-Haiyan soil had formed in a thin sand sheet, which has a composition similar to

the modern storm deposit and covers a second palaeosol at the base of the profiles (PE in Fig. 13a). It might be the deposit of a former storm.

In both washover fans, two successive sedimentary units were distinguished and investigated in detail for cores BAN 1–3 (transect 2; Figs 13b, S2). Unit 1 is massive to normally graded, composed of moderately sorted (1.5–2.6) medium sand (mean
5 = 250–320 µm) and shows a sharp boundary to the pre-Haiyan soil. It constitutes the entire typhoon layer in BAN 3, but is topped by a markedly thicker unit 2 in BAN 1 and 2. Unit 2 is composed of several planar to slightly inclined, normally or inversely graded beds of well-sorted (1.5–1.9) medium sand (mean = 300–480) with shell and coral fragments as well as pieces of litter. Both units contain >90% carbonates (aragonite and Mg-calcite). The Foraminifer assemblage is dominated by *Calcarina* sp. (32%), *Amphistegina* sp. (19%) and *Ammonia beccarii* (19%). Most of the tests are strongly reworked (<17%
10 fresh), though test preservation is much poorer (<1% fresh) in the palaeosol which is mainly composed of *Amphistegina* sp. (22%), *Ammonia beccarii* (21%), *Elphidium craticulatum* (12%) and *Quinqueloculina* spp. (12%). While unit 1 thins landwards in T3, neither a clear thinning tendency nor a fining trend is detectable in T2. Unit 2 is restricted to the proximal part of the washover fans (BAN 1–2, Figs 13, S2 and A–B, Fig. S1a) and rapidly thins landwards.

4.5 Inter-site comparison of sediment characteristics

15 ### 4.5.1 Geochemistry, mineralogy and foraminifers

The comparison of XRD data from all four sites reveals two general types of mineralogical compositions. While sediments from the carbonate environments (MOL, HER, BAN) are dominated by calcite, Mg-calcite and aragonite (at least 80%) with minor percentages of feldspar or quartz, the samples from the siliclastic coast (TOL) are mainly composed of feldspar and amphibole with a minor percentage of quartz (Fig. 8a).

20 A PCA on foraminifer data from the carbonate coasts indicates three PCs which explain 71% of the total variability. PC1 (44%) is characterized by positive loadings for the genera *Rosalina* sp., *Quinqueloculina* spp., *Peneroplis* sp., *Milionella* sp., *Globigerinoides* sp. and *Coscinospira* sp., while *Calcarina* and *Amphistegina* are negatively correlated. PC2 (15%) shows positive scores for *Amphistegina* sp. and strong reworking, and negative ones for *Heterostegina* sp. PC3 (12%) is positively correlated with *Challengerella* sp. and negatively with *Spirillina* sp. and *Schlumbergerella* sp. Plotting of PC1 against PC2
25 (Fig. S4, online supplement) reveals differences between sediment from the foreshore at Molocaboc (MOLsubtidal) on the one hand, and beach reference samples and storm deposits from all locations on the other. Differences between beach and storm deposits from different sites are less pronounced.

4.5.2 Granulometry

PCA combining granulometric data from all sites reveals three PCs that explain 82% of the total variability. Plotting of PC1
30 (positive loadings for mean, sorting, gravel and mode, negative ones for skewness and medium sand) versus PC2 (positive

loadings for mean, skewness and mode, negative ones for sorting and mud) reveal both site-dependent properties as well as distinct clusters for samples from units 1, units 2 and the palaeosols (Fig. 8b1).

In addition, PCAs on grain-size parameters were performed for each site separately. For TOL, PC1 (62.8%) and PC2 (33.5%) explain 96% of the total variability. Plotting of PC1 (positive loadings for skewness, mode and medium sand, negative ones for sorting and mud) versus PC2 (positive scores for sorting, mode and medium sand, negative ones for skewness) reveals clusters for unit 1, unit 2 and the pre-Haiyan soil (Fig. 8b3). Samples from HER reveal three PCs explaining 84% of the total variability. Plotting of PC1 (positive loadings for sorting, mud and fine sand, negative ones for skewness and coarse sand) versus PC2 (positive scores for fine and medium sand, negative ones for mode and sorting) reveals clustering of unit 1 and the palaeosol, while unit 2 forms two separate sample groups (HER 10 and all other profiles) (Fig. 8b2). At BAN, three PCs explain 86% of the total variation. Plotting of PC1 (positive loadings for mean, skewness and medium sand, negative ones for sorting and mud) versus PC2 (positive scores for mean, sorting, mode and gravel, negative ones for medium sand) reveals clusters for unit 1, unit 2 and the palaeosol, whereas reference samples from the upper and lower beach plot into the cluster of unit 2 (Fig. 8b4).

5. Discussion

5.1 Sedimentary footprint of Typhoon Haiyan on the Philippines

Based on eyewitness accounts and the interpretation of satellite images, most of the documented storm deposits can unambiguously be related to Typhoon Haiyan. Even at BAN A, where eyewitnesses report strong coastal erosion by tropical storm Basyang for the period between Haiyan and the field survey, satellite images from November 11th clearly document the formation of the washover fans by Typhoon Haiyan. Only at TOL, where both satellite images and eye witnesses cannot unambiguously relate all of the documented onshore deposits with Haiyan, the proximal parts of the washover sediments (unit 2 at TOL) cannot be excluded to be associated with post-Haiyan storm waves of Basyang. In addition to the fine-grained storm deposits reported in this study, Haiyan moved block- and boulder-sized reef-rock clasts at the coast of Eastern Samar, which have been discussed elsewhere (May et al., 2015b).

5.1.1 Sandy onshore deposits

Based on sedimentary and morphological criteria, the here presented sandy onshore deposits of extreme wave events are classified into (i) sand sheets and (ii) washover fans. The classification reflects different flooding regimes and, therefore, is assumed to represent hydrodynamic processes that lead to different sediment characteristics.

(i) Separated from the underlying soil by a layer of bended grass, the base of the typhoon deposits at TOL, HER, BAN B and MOL (the local units 1) is formed by normally graded or massive layers of sand. All sand sheets show comparably large inland

extents exceeding 100 m, are relatively thin (<10 cm), and exhibit landward fining and thinning trends (Fig. 3). Their appearance is similar to storm deposits formed under inundation regimes related to extensive flooding of back-barrier marshes described by Wang and Horwitz (2007). Indeed, complete inundation of coastal barriers and back-barrier areas at HER, TOL, BAN B and MOL is documented by flood marks. While at MOL and BAN B flooding is facilitated by the absence of a

5 pronounced beach ridge or by a nearby river mouth, flow depths of nearly 4 m a.s. and the complete submergence of barriers with crests more than 3 m a.s.l. at TOL and HER are either due to the high storm surge levels (TOL) or due to a combination of storm surge, high storm waves and related long-wave phenomena such as surf beat (HER) (Bricker et al., 2014; Kennedy et al., 2014; May et al., 2015b). The associated overland flow generally followed shore-perpendicular directions, if not re-directed by shore-parallel wall structures (TOL, Fig. 5). As indicated by scour marks (µCT scan of TOL 8, Fig. 7) and a rather

10 normally graded structure of these sand sheets, sediment dynamics related to this inundation regime (i.e., inundation overwash; cf. Donnelly et al., 2006) are – at least at TOL and HER – influenced by few tsunami-like flooding pulses due to infragravity waves with turbulent flow conditions during the peak of inundation (Mori et al., 2014; May et al., 2015b; Soria et al., 2015). Williams (2009) described very similar sediments for Hurricane Rita and dedicated them to deposition from suspension. Comparison of granulometry as well as foraminifer taphonomy and species composition with reference samples points to the

15 beach as the dominant sediment source (Figs 8b, S4). Nevertheless, the granulometry of the sand sheets shows slight differences to the modern beach, indicating a minor contribution of sediments from the foreshore or deeper water (Fig. 8b).

(ii) Unit 2 at TOL, HER, and BAN B, as well as the entire storm deposits at BAN A (the local units 1 and 2) are formed by lobate landforms of several decimetres thickness directly behind the barrier. As they (a) are restricted to the proximal part of back-barrier depressions (within <50 m from the shoreline), (b) form lobes with a gently inclined upper surface (1–5°) and a

20 steep landward front, (c) show multiple grading within horizontally to inclined laminated sections, and (d) reveal landward thinning and fining trends, these features resemble typical storm-induced washover fans, e.g. described by Sedgwick and Davis (2003), Phantuwongraj et al. (2013), or Williams (2015). They formed due to wave-induced sediment transport over the coastal barriers. This took place after the first flooding pulses inundated the coastal barriers, most likely during the peak of the storm surge when the largest storm waves occurred (Williams, 2009). So at TOL and BAN B, where the wind induced storm surge

25 was high, deposition is assumed to be caused by the swash of waves breaking at the inundated barrier. At HER, where the wind-induced storm surge was insufficient to inundate the coastal barrier and peak flooding levels were controlled by infragravity waves (i.e. at HER; May et al., 2015b), deposition was probably dominated by the swash of storm waves overtopping and scouring the not inundated barrier (i.e., run-up overwash; cf. Donnelly et al., 2006). Anyway, the washover fans they either form isolated structures such as at TOL, HER and BAN B, or coalescing washover terraces (BAN A). Since

30 breaching is associated with barrier erosion and radial spread of water and sediment into back-barrier depressions, granulometry and foraminifer taphonomy indicate that storm sediments were mainly derived from the beach and the coastal barrier (Figs 8b, S4). The swash of multiple individual waves generates successions of graded laminae which are probably

caused by gravity separation where a mixture of heavy minerals, quartz and shell fragments is present (TOL), or due to suspension settling of grain-size mixtures (HER, BAN A and B).

At site BAN A, where a basal sand sheet (unit 1 at TOL, BAN B and HER) is absent, flood marks indicate maximum water levels lower than the coastal barrier, and deposition is related to confined overwash. The internal stratification and washover morphology allow for a discrimination of a basal section with horizontal bedding associated with flat lobes (unit 1) and a section with steeply inclined layers with a steep avalanching front on top (unit 2). Horizontal lamination is interpreted as the result of initial barrier overtopping into dry back-barrier depressions associated with high flow velocities, whereas steep lobes with inclined bedding are associated with delta-front sedimentation into already flooded back-barrier depressions (Sedgwick and Davis, 2003; Switzer and Jones, 2008), e.g. due to high levels of the preceding storm surge or intensive rainfall.

5.1.2 Intertidal coral-rubble ridges

Considering the interviews with local fishermen and the fact that at least parts of the intertidal coral ridge at Carbin Reef in February 2014 covered reef organisms which must have been alive shortly before, formation or at least significant heightening can unambiguously be attributed to Typhoon Haiyan. Coral rubble ridges have repeatedly been reported to be a typical cyclone signature (Scheffers et al., 2012), e.g. on Funafuti Atoll, where Maragos et al. (1973) describe a cyclone-generated, intertidal coral ridge dominated by sand to boulder-sized rubble derived from the foreshore. Diving surveys before and after Haiyan revealed significant impact of the typhoon at the seaward reef slope while organisms on the intertidal platform were nearly untouched (Reyes et al., 2015), pointing to the entrainment of sediment from the foreshore and its deposition at the reef edge. Since ridge formation requires the repeated impact of breaking waves and wave swash is attenuated by the high porosity of rubble ridges (Spiske and Halley, 2014), ridge generation during Haiyan is mainly due to the impact of multiple storm waves breaking on top of the inundated reef platform.

The two morpho-sedimentary ridge units at Carbin may be explained as follows: (i) The entire ridge was formed by Typhoon Haiyan, whereas the distinct units reflect changing wind and wave directions. In accordance with a rotation of wind directions reported for the passage of Haiyan, unit 2 is present only at the W-exposed section of the ridge and may be interpreted as the result of stronger wind waves connected with increased destruction of the living reef at Carbin's slope as indicated by the fresh, angular coral fragments incorporated in unit 2. (ii) On the other hand, the more pronounced algae cover on coral rubble of unit 1 and the eyewitness accounts of ridge occurrence after Haiyan might also be explained by the impact of several typhoons. In this case, formation of the initial ridge (unit 1) would have taken place during former storms, while Haiyan only increased its height by adding fresh coral rubble on top (unit 2).

5.2 Spatial variability of fine-grained typhoon signatures

The spatial distribution and sedimentary structure of deposits formed by Typhoon Haiyan was critically influenced by both local setting and the hydrodynamic characteristics during inundation. Although onshore transport of sand is rather ubiquitous,

widespread sand sheets with a significant inland extent in the study area are restricted to locations with exceptional surge and/or inundation levels. This includes the exposed coastlines of Eastern Samar (HER) and the funnel-shaped San Pedro Bay (TOL), where a remarkable amplification of surge levels occurred during Haiyan (Mori et al., 2014). However, pressure and wind driven surge alone do not explain the high inundation levels, since models infer rather low surge levels of ~2 m,

5   particularly for Eastern Samar. While surge levels in the San Pedro Bay were additionally heightened by wave reflection in the enclosed embayment (Mori et al., 2014), the surprisingly high flooding levels along Eastern Samar are supposed to result from surf beat, caused by non-linear wave interactions with the fringing reef (Kennedy et al., 2014; May et al., 2015b).

On the other hand, washover features were even formed in areas with limited flooding levels and restricted landward inundation such as Bantayan and Northern Negros. Since washover deposits require high waves capable to overtop coastal barriers, their

10   local occurrence seems to be predetermined by bathymetry (river estuaries) and coastal morphology (pre-existing gaps or depressions in sandy barriers) as observed on Bantayan. Hence, they are limited to small sections of the coast even in heavily affected areas. For the localized occurrence of coral ridges on the reefs north of Negros, obligatory requirements seem to be (a) the presence of intertidal reef platforms with coral rubble in the foreshore zone; (b) exposure towards the main direction of the storm waves; and (c) waves high enough to entrain the foreshore sediment and to lift it onto the reef platform.

15   Local geology and geomorphology are also the main factors determining the composition of the investigated typhoon deposits (Fig. 8). (i) Variations of total sediment composition (mineralogy and granulometry) between different sites are more significant than variations between different units at individual sites (Fig. 8a, b). The granulometry of storm-transported sediment varies with the sediment availability at the beach and the foreshore zone so that dominant grain size varies between HER, TOL and BAN (Fig. 8b). Geochemistry and mineralogy basically reflect differences between siliciclastic and carbonate

20   coasts (Fig. 8a). Likewise, clearly laminated washover deposits (alternation of dark and light laminae) are linked to the presence of heavy minerals at siliciclastic coastlines (TOL), while bedding structures are less prominent in carbonate environments (BAN and HER). (ii) On an intra-site level, mineralogy and geochemistry (due to insignificant differences) and microfauna (due to a limited dataset) only allow for a separation between storm deposits and underlying palaeosols, while sedimentary structures and grain-size data enable further discrimination of distinct subunits (Fig. 8b). Although reference data from recent

25   environments are very limited, granulometric differences between consecutive sublayers of the storm deposit seem to be related to varying sediment sources (beach vs. foreshore) and different hydrodynamic transport conditions as described by Switzer and Jones (2008). This is the case for the units 1 and 2 at sites TOL, HER and BAN (Fig. 8b), while the large scatter within the unit 2 deposits at HER might be explained by deposition of the HER 10 deposits by backwash, since the core was taken close to a backflow channel.

30   **5.3 Implications for palaeotempestology**

Since the sedimentary characteristics of Typhoon Haiyan's deposits show significant site-specific variations, it is not possible to infer one particular storm signature type. Nevertheless, storm deposits can clearly be distinguished from most other

depositional processes on the basis of granulometry, internal structures, mineralogy or faunal composition. Only tsunamis are capable to produce similar features, due to comparable hydrodynamic characteristics that potentially allow for barrier overwash, landward transport of sand for hundreds of meters, and the generation of waves strong enough to entrain and lift subtidal coral rubble onto intertidal reef platforms (Shanmugam, 2012). Unfortunately, only very few tsunami signatures that

5   might facilitate discrimination (e.g. Morton et al., 2007) have been described for the Philippines (Imamura et al., 1995). Hence, it is not possible to evaluate which of the sedimentary characteristics documented in this study are unique for the impact of local typhoons.

So far, coral ridges have been reported to be exclusively generated by cyclones (Scheffers et al., 2012), which seems straightforward. Ridge formation requires repeated breaking waves as observed during cyclones (Nott, 2006), while the small

10   number of inundation pulses characteristic for tsunamis tends to produce randomly scattered boulder fields (Richmond et al., 2011; Weiss, 2012). However, preservation of coral ridges is often limited (Baines and McLean,1976), and age determination remains challenging due to potential reworking of the components (Scheffers et al., 2014). On the other hand, sand sheets with large inland extents are typical signatures of tsunamis as well (e.g. Jankaew et al., 2008), and washover fans with internal lamination have been reported for both types of deposits (Switzer et al., 2012; Atwater et al., 2013).

15   Nevertheless, Haiyan and its sedimentary record offer some valuable considerations regarding the interpretation of palaeoevent deposits in geological records both in the Philippines (e.g. for the young palaeoevents documented on Bantayan) and in general. While the composition and granulometry of sand sheets related to storm inundation are controlled by local geology, and landward thinning and fining trends are similar to those observed in tsunami deposits (Goto et al., 2008), the inland extent of the Haiyan-laid sand sheets presented here is limited compared to sandy deposits of many recent tsunamis with comparable

20   inundation levels (e.g., Hawkes et al., 2007; Goto et al., 2011). This is true even at sites with onshore flooding levels >5 m a.s.l. such as at HER and TOL. Although the landward limit of coastal inundation may be confined by mud deposits rather than by sand layers (e.g., Williams, 2010; Abe et al., 2012; Goto et al., 2014), our findings seem to corroborate previous conclusions that the landward extent of tsunami sand sheets in low lying coasts tends to be larger in comparison with sandy storm deposits (cf. Morton et al., 2007). On the other hand, the combined occurrence of (i) a thin (i.e., a few cm), massive or

25   graded basal unit formed due to surge-related extensive coastal flooding (unit 1 at TOL and HER), and (ii) a laminated, swash-induced, spatially limited washover unit on top (unit 2 at TOL, BAN B and HER, units 1 and 2 at BAN A) that in case of HER can both be related to Haiyan and therefore a single storm event, might be rather indicative for cyclone-generated deposition. However, at TOL part of this succession (i.e. the washover unit on top) could also be the result of deposition by Basyang so that the association of the two units might also be explained by several storm events in a quick sequence; in this case the strong

30   beach erosion during a major event such as Supertyphoon Haiyan seems to increase the susceptibility of the sedimentary coastline towards storm overwash.

6. Conclusions

The geological imprint of Typhoon Haiyan is strongly influenced by local factors causing a wide variety of site-specific sedimentary and morphological characteristics. Nevertheless, in spite of their spatial variability, Haiyan's geological legacy exhibits several typical storm-related depositional patterns – including washover fans, extensive sand sheets and coral rubble ridges – that can be related to specific hydrodynamic processes and depositional environments.

Massive to normally graded onshore sand sheets extend 100–300 m inland, tend to fine and thin landwards, and are related to widespread inundation of coastal lowlands and complete submergence of the coastal barrier. They have formed in areas of significant amplification of the storm surge. In contrast, washover fans are composed of small (10–50 m inland) sand lobes with steep landward fronts and a distinct internal stratification that occur localized behind breaches or depressions in coastal barriers as the result of overtopping waves and repeated overwash. Coral rubble ridges were formed on intertidal reef platforms by storm waves entraining coral fragments from the reef slope and breaking at the reef edge.

Since Haiyan was one of the most powerful cyclones ever recorded, these and other findings from the Philippines particularly add to the general knowledge of extreme wave deposits and, ultimately, may contribute to discriminating sediments of strong cyclones and tsunamis. While coral rubble ridges so far seem to be a unique feature of strong storms, the sandy onshore deposits left by Haiyan are very similar to those generated by tsunamis. However, the inland extents of sand sheets documented in this study are significantly smaller compared to those of large tsunamis with comparable flooding levels. Although more extensive sand layers have been reported for other TC and moderate tsunamis generate sand sheets in the range of the Haiyan deposits, the inland extent of onshore sand sheets at least provides a valuable tendency for the discrimination of cyclones and strong tsunamis. In addition, the combined occurrence of basal sand sheets and overlying confined and well-stratified sand units may be indicative for cyclones, since they result from the succession of surge-related extensive coastal inundation and subsequent wave overwash during Haiyan at HER, which is not known to be typical for tsunamis. But the ambiguous origin of the respective units at TOL, where they might as well result from two successive storms, prevents a more definite conclusion.

Acknowledgements

This research was financially supported by the Faculty of Mathematics and Natural Sciences, University of Cologne (UoC), and a UoC Postdoc Grant. Invaluable logistic support was provided by Karen Tiopes and Verna Vargas (Department of Tourism, Leyte Branch). We are very thankful for the great hospitality throughout the Visayas archipelago and the first-hand insights provided by local interviewees, which is even more admirable considering the trauma after the disaster. Ramil Villaflor is acknowledged for guiding us safely through the islets north of Negros.

References

Abe, T., Goto, K., and Sugawara, D.: Relationship between the maximum extent of tsunami sand and the inundation limit of the 2011 Tohoku-oki tsunami on the Sendai Plain, Japan, Sed Geol, 282, 142–150, 2012.

Atwater, B.F., Cisternas, M., Yulianto, E., Prendergast, A.L., Jankaew, K., Eipert, A.A., Starin Fernando, W.I., Tejakusuma, I., Schiappacasse, I., and Sawai, Y.: The 1960 tsunami on beach-ridge plains near Maullín, Chile: Landward descent, renewed breaches, aggraded fans, multiple predecessors, Andean Geol, 40, 393–418, 2013.

Baines, G.B.K. and McLean, R.F.: Sequential studies of hurricane deposit evolution at Funafuti Atoll, Mar Geol, 21, 1–8, 1976.

Bird, E.C.F.: Philippines. In: Encyclopedia of the World's Coastal Landforms, Springer, Dordrecht, 1151–1156, 2010.

Bishop, P., Sanderson, D., Hansom, J., and Chaimanee, N.: Age-dating of tsunami deposits: lessons from the 26 December 2004 tsunami in Thailand, Geogr J, 171, 379–384, 2005.

Blott, S.J. and Pye, K.: GRADISTAT: A grain size distribution and statistics package for the analysis of unconsolidated sediments, Earth Surf Proc Land, 26, 1237–1248, 2001.

Bricker, J., Takagi, H., Mas, E., Kure, S., Adriano, B., Yi, C., and Roeber, V.: Spatial variation of damage due to storm surge and waves during Typhoon Haiyan in the Philippines, J Japan Soc Civil Eng Ser, 70(2), 231–235, 2014.

Brill, D., Klasen, N., Brückner, H., Jankaew, K., Scheffers, A., Kelletat, D., and Scheffers, S.: OSL dating of tsunami deposits from Phra Thong Island, Thailand, Quat Geochronol, 10, 224–229, 2012.

Brill, D., Pint, A., Jankaew, K., Frenzel, P., Schwarzer, K., Vött, A., and Brückner, H.: Sediment transport and hydrodynamic parameters of tsunami waves recorded in onshore geoarchives – A case study from Thailand, J Coastal Res, 30, 922–941, 2014.

Brückner, H. and Brill, D.: Der Tsunami von 2004 – fünf Jahre danach, Geogr Rundsch, 61(12), 4–10, 2009.

Corral, A., Ossó, A., and Llebot, J.E.: Scaling of tropical-cyclone dissipation, Nat Phys, 6, 693–696, 2010.

Cuadra, C., Biton, N.I., Cabacaba, K.M., Santiago, J., Suarez, J.K., Lapidez, J.P., Lagmay, A.M.F., and Malano, V.: Development of Inundation Map for Bantayan Island, Cebu Using Delft3D-Flow Storm Surge Simulations of Typhoon Haiyan, NOAH Open-File Reports, 3, 37–44, 2014.

Dimalanta, C.B., Suerte, L.O., Yumul, G.P., Tamayo, R.A., and Ramos, E.G.L.: A Cretaceous supra-subduction oceanic basin source for Central Philippine ophiolitic basement complexes: Geological and geophysical constraints, Geosci J, 10(3), 305–320.

Donnelly, C., Kraus, N., and Larson, M.: State of knowledge on the measurement and modeling of coastal overwash, J Coastal Res, 22, 965-991, 2006.

Engel, M., Brill, D., May, S.M., Brückner, H., and Reyes, M.: Philippinen: "Haiyans" Erbe, Geogr Rundsch, 66(6), 54–57, 2014.

Folk, R.L. and Ward, W.C.: Brazos River bar: a study in the significance of grain size parameters, J Sediment Petrol, 27, 3–26, 1957.

Fritz, H.M., Blount, C.D., Thwin, S., Kyaw Thu, M., and Chan, N.: Cyclone Nargis storm surge in Myanmar, Nat Geosci, 2, 448–449, 2009.

Goto, K., Imamura, F., Keerthi, N., Kunthasap, P., Matsui, T., Minoura, K., Ruangrassamee, A., Sugawara, D., and Supharatid, S.: Distribution and significance of the 2004 Indian Ocean tsunami deposits: Initial results from Thailand and Sri Lanka. In: Tsunamiites. Features and Implications, Elsevier, Amsterdam, Oxford, 105–122, 2008.

Goto, K., Chague-Goff, C., Fujino, S., Goff, J., Jaffe, B., Nishimura, Y., Richmond, B., Sugawara, D., Szczucinski, W., Tappin, D.R., Witter, R., and Yulianto, E.: New insights of tsunami hazard from the 2011 Tohoku-oki event, Mar Geol, 290, 46–50, 2011.

Goto, K., Hashimoto, K., Sugawara, D., Yanagisawa, H., and Abe, T.: Spatial thickness variability of the 2011 Tohoku-oki tsunami deposits along the coastline of Sendai Bay, Mar Geol, 358, 38–48, 2014.

Hammer, Ø., Harper, D.A.T., and Ryan, P.D.: PAST: Paleontological statistics software package for education and data analysis, Palaeontol Electron 4(1), article 4, 2001.

Hawkes, A.D., Bird, M., Cowie, S., Grundy-Warr, C., Horton, BP., Tan Shau Hwai, A., Law, L., Macgregor, C., Eong Ong, J., Rigg, J., Robinson, R., Tan-Mullins, M., Tiong Sa, T., Yasin, Z., and Wan Aik, L.: Sediments deposited by the 2004 Indian Ocean Tsunami along the Malaysia–Thailand Peninsula, Mar Geol, 242, 169–190, 2007.

Hippensteel, S.P., Eastin, M.D., and Garcia, W.J.: The geological legacy of Hurricane Irene: Implications for the fidelity of the paleo-storm record, GSA Today, 23(12), 4–10, 2013.

Imamura, F., Synolakis, C.E., Gica, E., Titov, V., Listanco, E., and Lee, H.J.: Field survey of the 1994 Mindoro Island, Philippines tsunami, Pure Appl Geophys, 144(3-4), 875–890, 1995.

International Research Institute of Disaster Science, IRIDeS: Initial Report of IRIDeS fact-finding mission to Philippines. TOHOKU University, 2014. Http://irides.tohoku.ac.jp/media/files/IRIDeS_Report_Haiyan_20140527.pdf. Last access on 05/31/2015.

Jankaew, K., Atwater, B.F., Sawai, Y., Choowong, M., Charoentitirat, T., Martin, M.E., and Prendergast, A.: Medieval forewarning of the 2004 Indian Ocean tsunami in Thailand, Nature, 455, 1228–1231, 2008.

Kennedy, A., Mori, N., Zhang, Y., Tajima, Y., Pecor, W., Yasuda, T., Chen, S.-E., Nakamura, S., and Cruz, E.: Onshore Transport of Large Nearshore Boulders during Super Typhoon Haiyan, AGU Fall Meeting, San Francisco, 15–19 Dec 2014, Abstract OS23C-1232, 2014.

Knutson, T.R., McBride, J.L., Chan, J., Emanuel, K., Holland, G., Landsea, C., Held, I., Kossin, J.P., Srivastava, A.K., and
5   Sugi, M.: Tropical cyclones and climate change, Nat Geosci, 3, 157–163, 2010.

Kortekaas, S., and Dawson, A.G.: Distinguishing tsunami and storm deposits: An example from Martinhal, SW Portugal, Sediment Geol, 200, 208–221, 2007.

Lagmay, A.M.F., Agaton, R.P., Bahala, M.A.C., Briones, J.B.L.T., Cabacaba, K.M.C., Caro, C.V.C., Dasallas, L.L., Gonzalo, L.A.L., Ladiero, C.N., Lapidez, J.P., Mungcal, M.T.F., Puno, J.V.R., Ramos, M.M.A.C., Santiago, J., Suarez, J.K., and
10 Tablazon, J.P.: Devastating storm surges of Typhoon Haiyan, Int J Disaster Risk Red, 11, 1–12, 2015.

Maragos, J.E., Baines, G.B.K., and Beveridge, P.J.: Tropical Cyclone Bebe creates a new land formation on Funafuti Atoll, Science, 181, 1161–1164, 1973.

Mas, E., Bricker, J., Kure, S., Adriano, B., Yi, C., Suppasri, A., and Koshimura, S.: Field survey report and satellite image interpretation of the 2013 Super Typhoon Haiyan in the Philippines, Nat Hazard Earth Sys, 15, 805–816, 2015.

15 Matias, A., Ferreira, Ó., Vila-Concejo, A., Garcia, T., Dias, J.A.: Classification of washover dynamics in barrier islands, Geomorphology, 97, 655–674, 2010.

May, S.M., Engel, M., Brill, D., Squire, P., Scheffers, A., Kelletat, D.: Coastal hazards from tropical cyclones and extratropical winter storms based on Holocene storm chronologies. In: Coastal Hazards, Springer, 557–585, 2013.

May, S.M., Brill, D., Engel, M., Scheffers, A., Pint, A., Opitz, S., Wennrich, V., Squire, P., Kelletat, D., Brückner, H.: Traces
20 of historical tropical cyclones and tsunamis in the Ashburton Delta (NW Australia), Sedimentology. doi:10.1111/sed.12192, 2015a.

May, S.M., Engel, M., Brill, D., Cuadra, C., Lagmay, A.M.F., Santiago, J., Suarez, J.K., Reyes, M., and Brückner, H.: Block and boulder transport in Eastern Samar (Philippines) during Supertyphoon Haiyan, Earth Surface Dynamics, 3, 543-558, 2015b.

25 Morgerman, J.: Super Typhoon Haiyan in Tacloban City & Leyte, Philippines, iCyclone Chase Report, 2014.

Mori, N., Kato, M., Kim, S., Mase, H., Shibutani, Y., Takemi, T., Tsuboki, K., and Yasuda, T.: Local amplification of storm surge by Super Typhoon Haiyan in Leyte Gulf, Geophys Res Lett, 41(14), 5106–5113, 2014.

Morton, R., Gelfenbaum, G., and Jaffe, B.: Physical criteria for distinguishing sandy tsunami and storm deposits using modern examples, Sediment Geol, 200, 184–207, 2007.

Nanayama, F., Shigeno, K., Satake, K., Shimokawa, K., Koitabashi, S., Miyasaka, S., and Ishii, M.: Sedimentary differences between the 1993 Hokkaido-nansei-oki tsunami and the 1959 Miyakojima typhoon at Taisei, southwestern Hokkaido, northern Japan, Sediment Geol, 135, 255–264, 2000.

Navy METOC: http://www.metoc.gov.au/ArcGIS/rest/services/climatology/significant_wave_height/MapServer, 2014. Last access on 11/14/2014.

NDRRMC: SitRep No. 107 Effects of Typhoon "YOLANDA" (HAIYAN) (14 March 2014), http://www.ndrrmc.gov.ph/attachments/article/1125/Update%20Yolanda%20Sitrep%20107.pdf, 2014. Last access on 03/19/2014

Nott, J.: Tropical cyclones and the evolution of the sedimentary coast of Northern Australia, J Coastal Res, 22, 49–62, 2006.

PAGASA: Climate change in the Philippines, Climatology and Agrometeorology Division, 2011.

PAGASA: Storm surge occurences during the passage of Typhoon Yolanda on November 8, 2013 in selected areas of Leyte and Samar, Report of PAGASA Stride team, 2014.

Phantuwongraj, S., Choowong, M., Nanayama, F., Hisada, K.-I., Charusiri, P., Chutakositkanon, V., Pailoplee, S., and Chabangbon, A.: Coastal geomorphic conditions and styles of storm surge washover deposits from Southern Thailand, Geomorphology, 192, 43-58, 2013.

Pun, I.F., Lin, I.I., and Lo, M.H.: Recent increase in high tropical cyclone heat potential area in the Western North Pacific Ocean, Geophys Res Lett, 40, 4680–4684, 2013.

Rangin, C., Müller, C., and Porth, H.: Neogene geodynamic evolution of the Visayan Region, Geol Jahrb, Reihe B, 70, 7–27, 1989.

Reyes, M., Engel, M., May, S.M., Brill, D., and Brückner, H.: Life and death after Super Typhoon Haiyan, Coral Reefs, 34, 419, 2015.

Richmond, B.M., Watt, S., Buckley, M., Jaffe, B., Gelfenbaum, G., and Morton, R.A.: Recent storm and tsunami coarse-clast deposit characteristics, southeast Hawaii, Mare Geol, 283, 79-89, 2011.

Scheffers, A., Engel, M., Scheffers, S., Squire, P., and Kelletat, D.: Beach ridge systems – archives for Holocene coastal events? Prog Phys Geog, 36, 5–37, 2012.

Scheffers, A.M., Engel, M., May, S.M., Scheffers, S.R., Joannes-Boyau, R., Hänßler, E., Kennedy, K., Kelletat, D., Brückner, H., Vött, A., Schellmann, G., Schäbitz, F., Radtke, U., Sommer, B., Willershäuser, T., and Felis, T.: Potential and limits of combining studies of coarse and fine-grained sediments for the coastal event history of a Caribbean carbonate environment, Geol Soc London Spec Publ, 388, 503–531, 2014.

Schwartz, R.K.: Bedform and stratification characteristics of some modern small-scale washover sand bodies, Sedimentology, 29, 835–849, 1982.

Sedgwick, P.E. and Davis, R.A.: Stratigraphy of washover deposits in Florida: implications for recognition in the stratigraphic record, Mar Geol, 200, 31–48, 2003.

5 Shanmugam, G.: Process-sedimentological challenges in distinguishing paleo-tsunami deposits, Nat Hazards, 63, 5–30, 2012.

Soria, J.L., Switzer, A., Villanoy, C., Fritz, H., Bilgera, P.H., Cabrera, O., Siringan, F., Sta. Maria, Y., Ramos, R., and Fernandez, I.: Repeat storm surge disasters of Typhoon Haiyan and its 1897 predecessor in the Philippines, Bulletin of the American Meteorological Society, 97, 31–48, 2015.

Spiske, M. and Halley, R.B.: A coral-rubble ridge as evidence for hurricane overwash, Anegada (British Virgin Islands), Adv
10 Geosci, 38, 9–20, 2014.

Switzer, A.D. and Jones, B.G.: Setup, deposition, and sedimentary characteristics of two storm overwash deposits, Abrahams Bosom Beach, southeastern Australia, J Coastal Res, 24, 189–200, 2008.

Switzer, A., Srinivasalu, S., Thangadurai, N., and Ram Mohan, V.: Bedding structures in the Indian tsunami deposits that provide clues to the dynamics of tsunami inundation, Geol Soc London Spec Publ, 361, 61–77, 2012.

15 Tajima, Y., Yasuda, T., Pacheco, B.M., Cruz, E.C., Kawasaki, K., Nobuoka, H., Miyamoto, M., Asano, Y., Arikawa, T., Ortigas, N.M., Aquino, R., Mata, W., Valdez, J., and Briones, F.: Initial report of JSCE-PICE joint survey on the storm surge disaster caused by Typhoon Haiyan, Coast Eng J, 56(1), 14500065, 2014.

Wang, P. and Horwitz, M.H.: Erosional and depositional characteristics of regional overwash deposits caused by multiple hurricanes, Sedimentology, 54, 545–564, 2007.

20 Weiss, R.: The mystery of boulders moved by tsunamis and storms, Mar Geol, 295–298, 28–33, 2012.

Williams, H.F.L.: Stratigraphy, sedimentology and microfossil content of Hurricane Rita storm surge deposits in Southwest Louisiana, J Coastal Res, 25, 1041-1051, 2009.

Williams, H.F.L.: Storm surge deposition by Hurricane Ike on the McFaddin National Wildlife Refuge, Texas: Implications for palaeotempestology studies, J Foramin Res, 40, 210–219, 2010.

25 Williams, H.F.L.: Contrasting styles of Hurricane Irene washover sedimentation on three east coast barrier islands: Cape Lookout, North Carolina; Assateague Island, Virginia; and Fire Island, New York, Geomorphology, 231, 182–192, 2015.
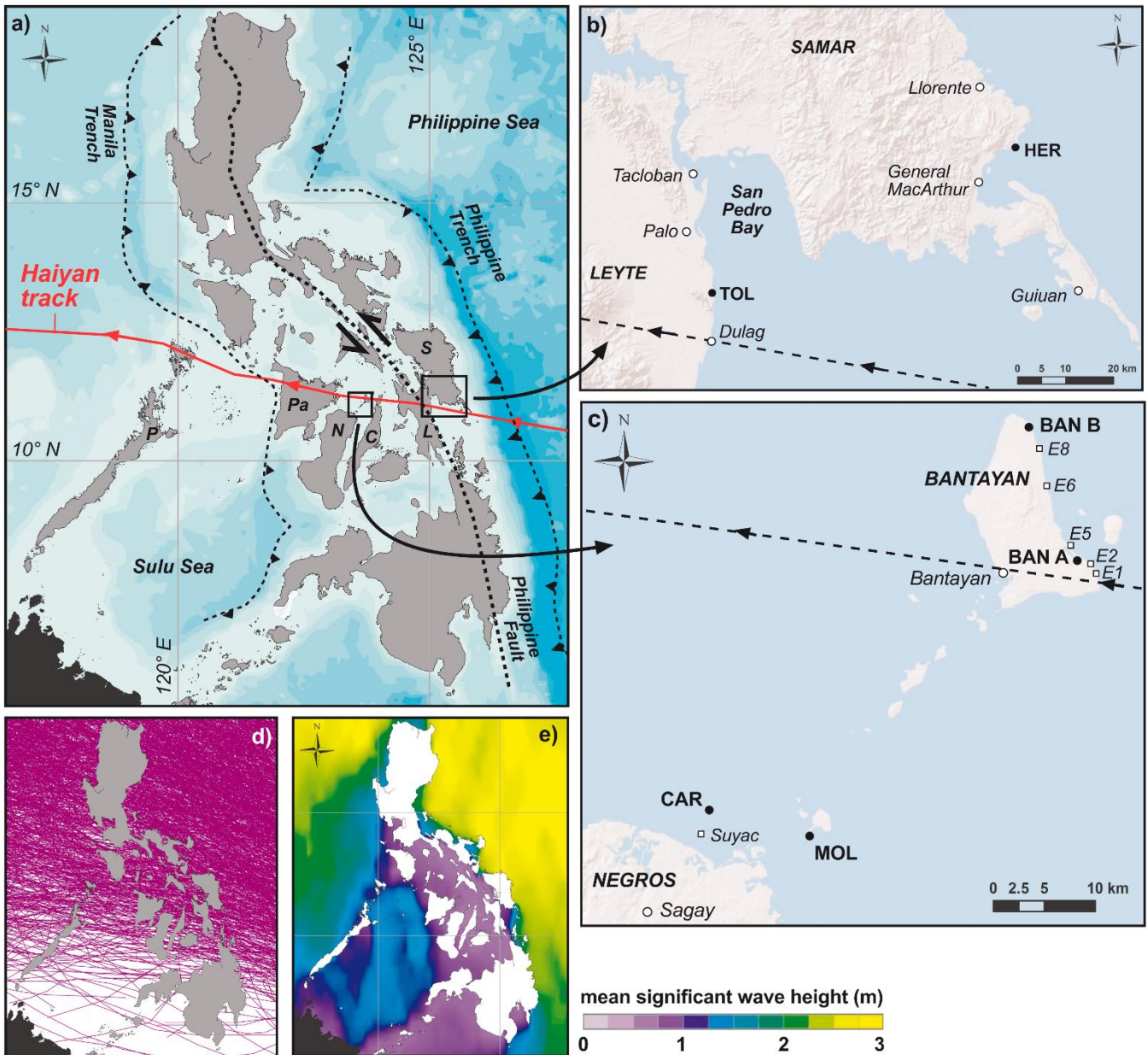
Fig. 1: Overview of the study area. a) Philippine archipelago with main tectonic structures (Rangin et al. 1989), track of Typhoon Haiyan (NDRRMC 2014), and position of research areas on Samar and Leyte (b), as well as northern Negros and Bantayan (c) (based on ESRI basemaps). S – Samar, L – Leyte, C – Cebu, N – Negros, Pa – Panay, P – Palawan. d) Historical cyclone tracks
5 **crossing the Philippines since the beginning of weather recording (NOAA Historical Hurricane Track Pool) illustrate a decreasing cyclone frequency from north to south. e) Mean significant wave heights (Navy METOC 2014) indicate highest wave energy during winter monsoon along the exposed east coasts and usually calm conditions in the interior parts of the archipelago.**
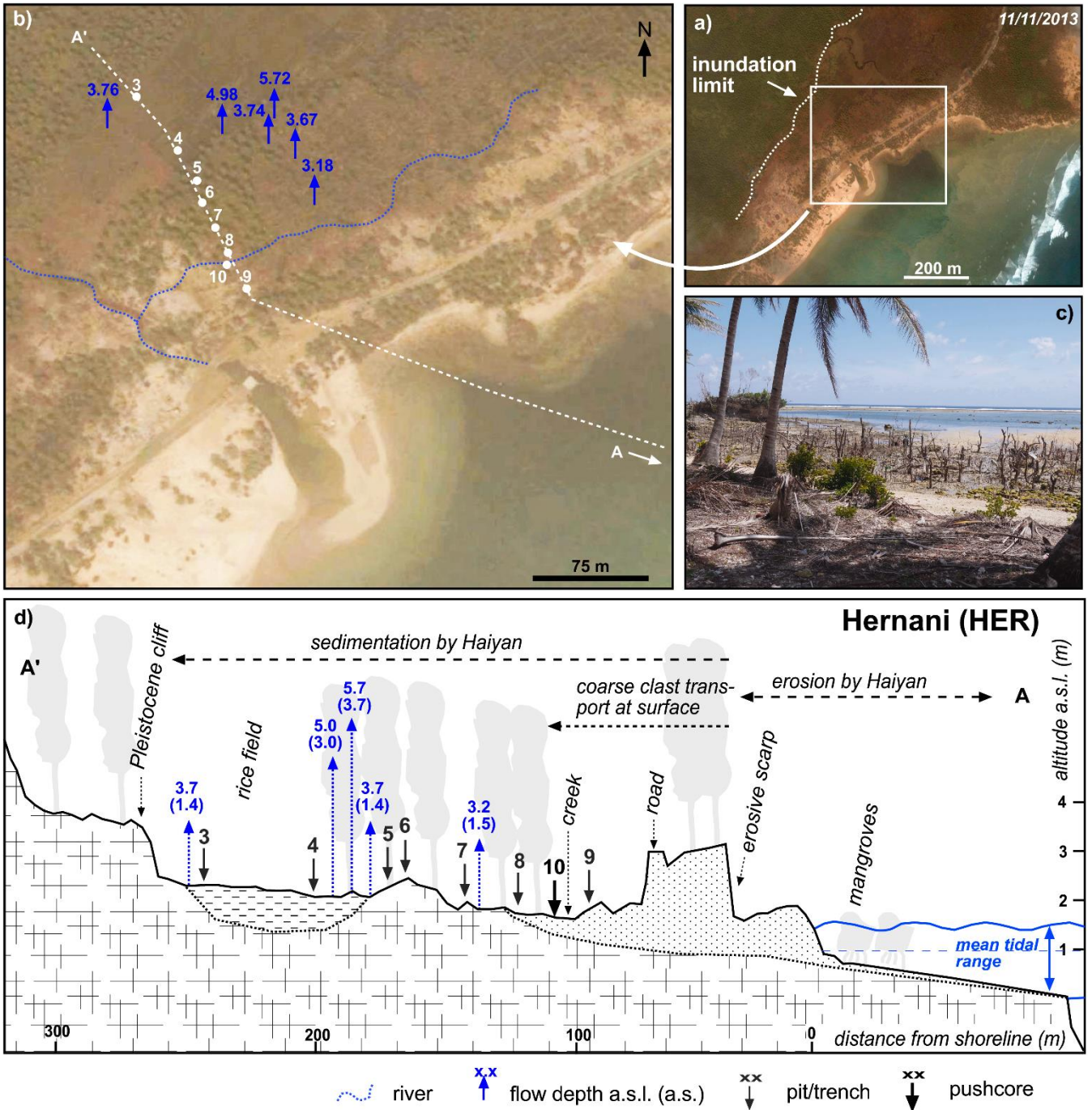
Fig. 2: Hernani (HER) study site with documented Haiyan flood marks and positions of sampled typhoon deposits. a) Local Typhoon Haiyan inundation limit (based on Google Earth/Digital Globe 11/11/2013). b) Onshore sediments were investigated along a coast-perpendicular transect (A–A') crossing the flooded area. c) Destroyed mangroves in front of the beach (view from the shore-parallel main road, photography: February 2014). d) Topographical cross section (A–A') with sampling sites. With water levels of more than 5 m a.s.l. flooding during Haiyan overtopped the sandy coastal barrier, destroyed the road on its top, and transported sand nearly 300 m inland to the foot of the former cliff.
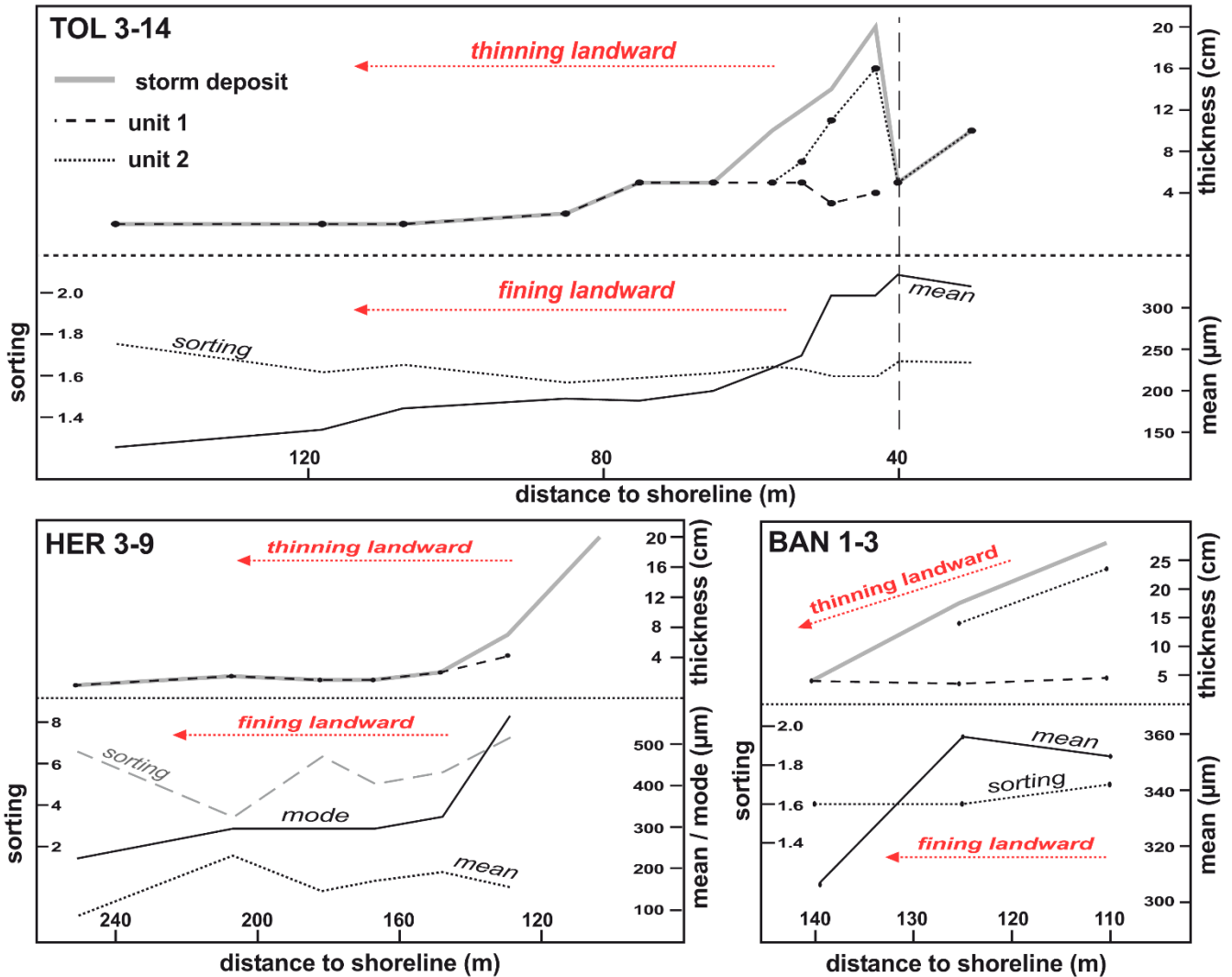
Fig. 3: Coast-perpendicular trends of grain size and thickness in typhoon deposits. Onshore deposits at sites TOL, HER and BAN B tend to thin and fine landward, while no clear trend in sorting was detected. Note the different scales.
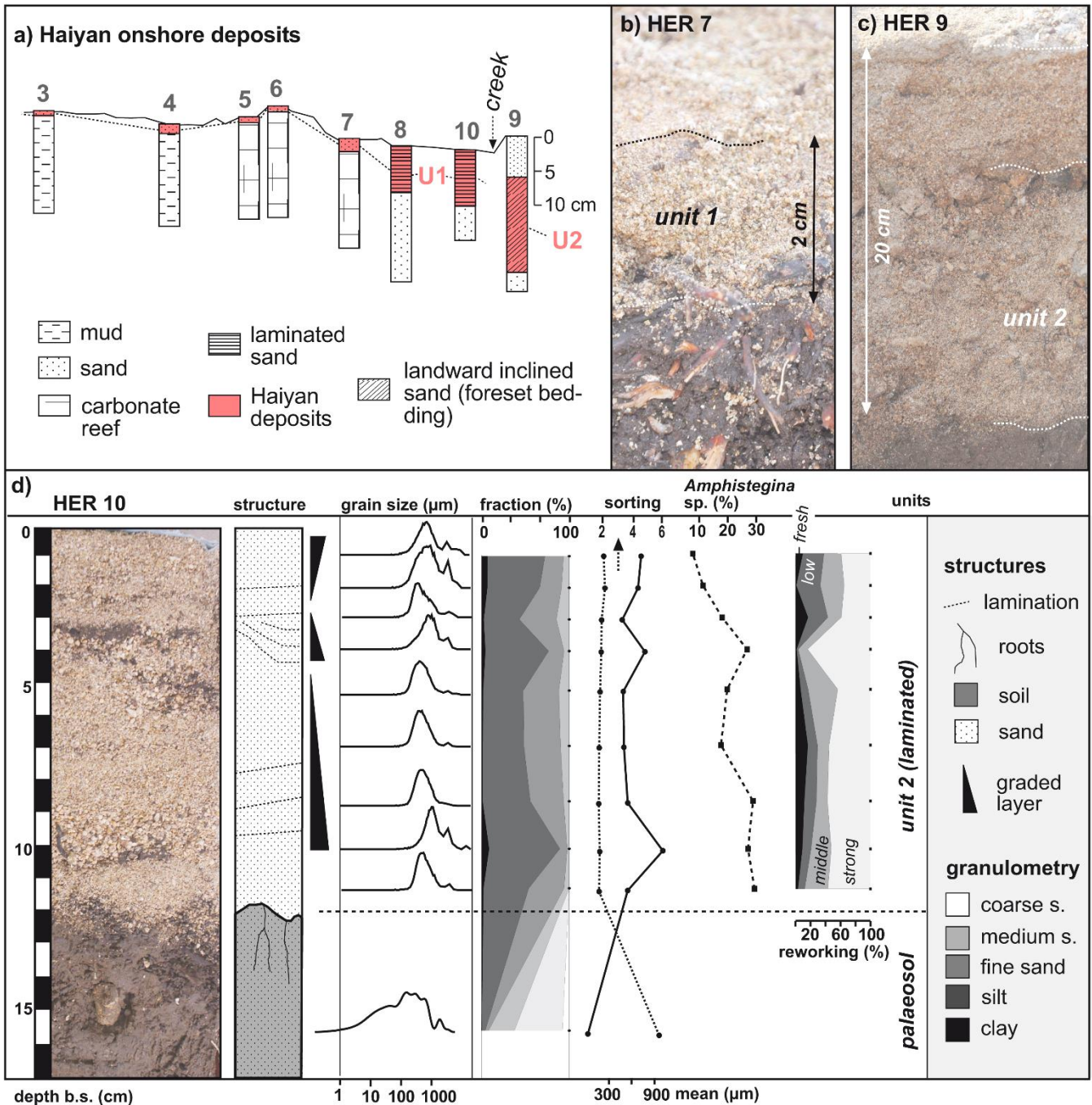
Fig. 4: **Onshore deposits of Typhoon Haiyan at site HER. a) Coast-perpendicular transect illustrating the succession of typhoon deposits (see Fig. 2 for location). The basal unit 1 (U1) continuously thins landwards, while unit 2 (U2) is restricted to the proximal part of the coastal plain (HER 8–10). b) The 2 cm thick unit 1 at HER 7 (photography: February 2014). c) The 20 cm thick unit 2 at HER 9 (photography: February 2014). d) Sedimentary characteristics of HER 10. A 12 cm thick typhoon layer can clearly be separated from the palaeosol. The storm layer reveals repeated normally and inversely graded laminae, in which the amount of strongly reworked foraminifera is highest within the coarse basal sections.**

2016-07-04
10.5194/nhess-2016-224
journal article
en
Author(s) 2016. CC-BY 3.0 License.
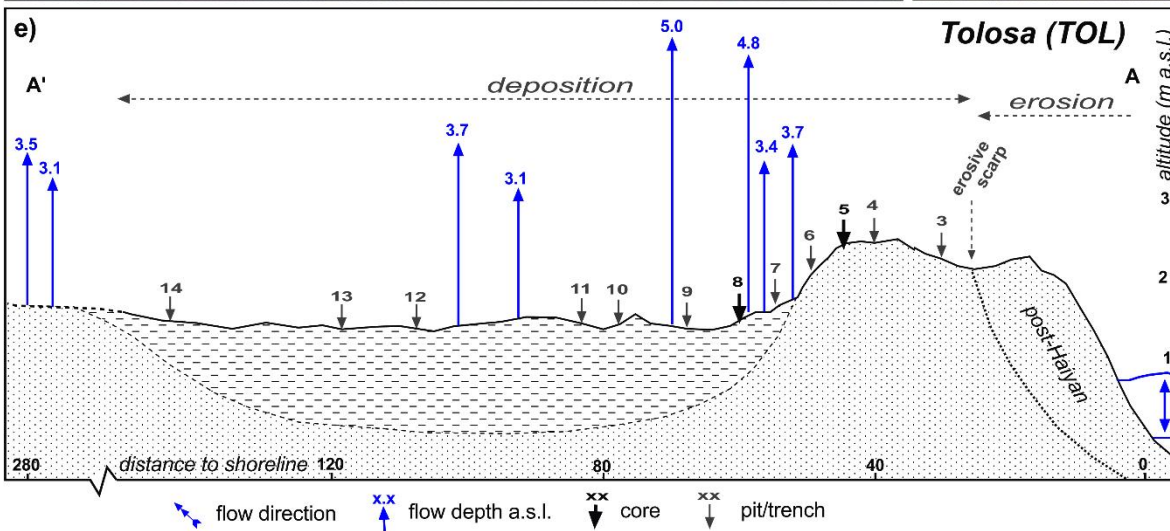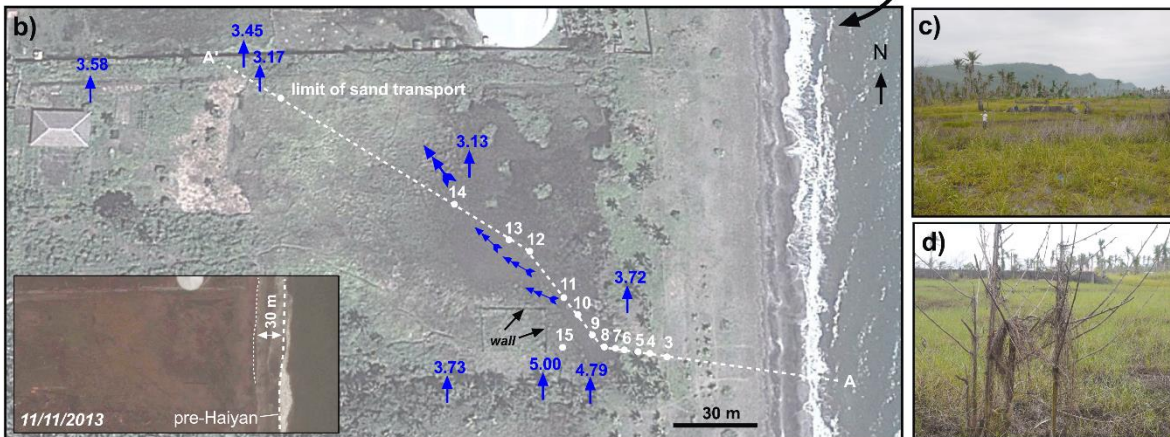
Fig. 5: Tolosa (TOL) study site with documented Haiyan flood marks and positions of sampled typhoon deposits. a) Local inundation limit reached several 100 metres inland (based on Google Earth/Digital Globe 11/11/2013, i.e. immediately after Haiyan). b) Onshore sediments were investigated along a coast-perpendicular transect (A–A') crossing the inundated area (based on Google Earth/Digital Globe 02/23/2012; insert: Google Earth 11/11/2013). c) Westward view from the beach ridge over the back-barrier marsh. d) Flood debris in bushes served as an indicator for flow depth. e) With flow levels of up to 5 m a.s.l., Haiyan flooded the beach ridge entirely and transported sand nearly 300 m inland.
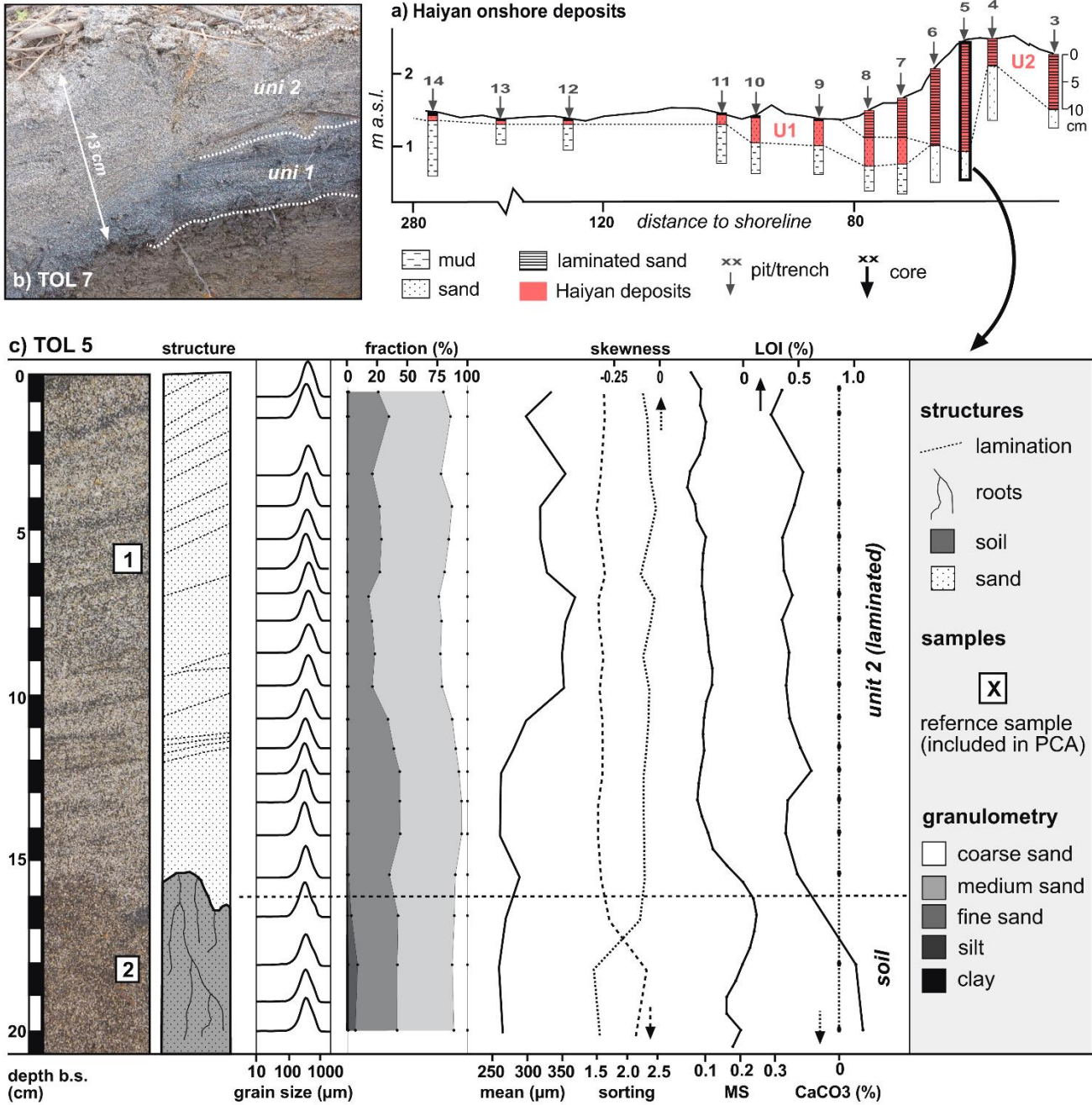
Fig. 6: Typhoon Haiyan onshore deposits at site TOL. a) Coast-perpendicular transect illustrating the succession of typhoon deposits. A graded to massive basal unit (U1) is covered by a laminated unit (U2) in the proximal part of the coastal plain (TOL 3–8). b) The 10 cm thick deposit at TOL 7 consists of massive sand at the base (unit 1) and laminated sand on top (unit 2). c) Sedimentary characteristics of TOL 5. The 16 cm thick, laminated typhoon layer can clearly be separated from the palaeosol due to lower LOI and magnetic susceptibility (MS).
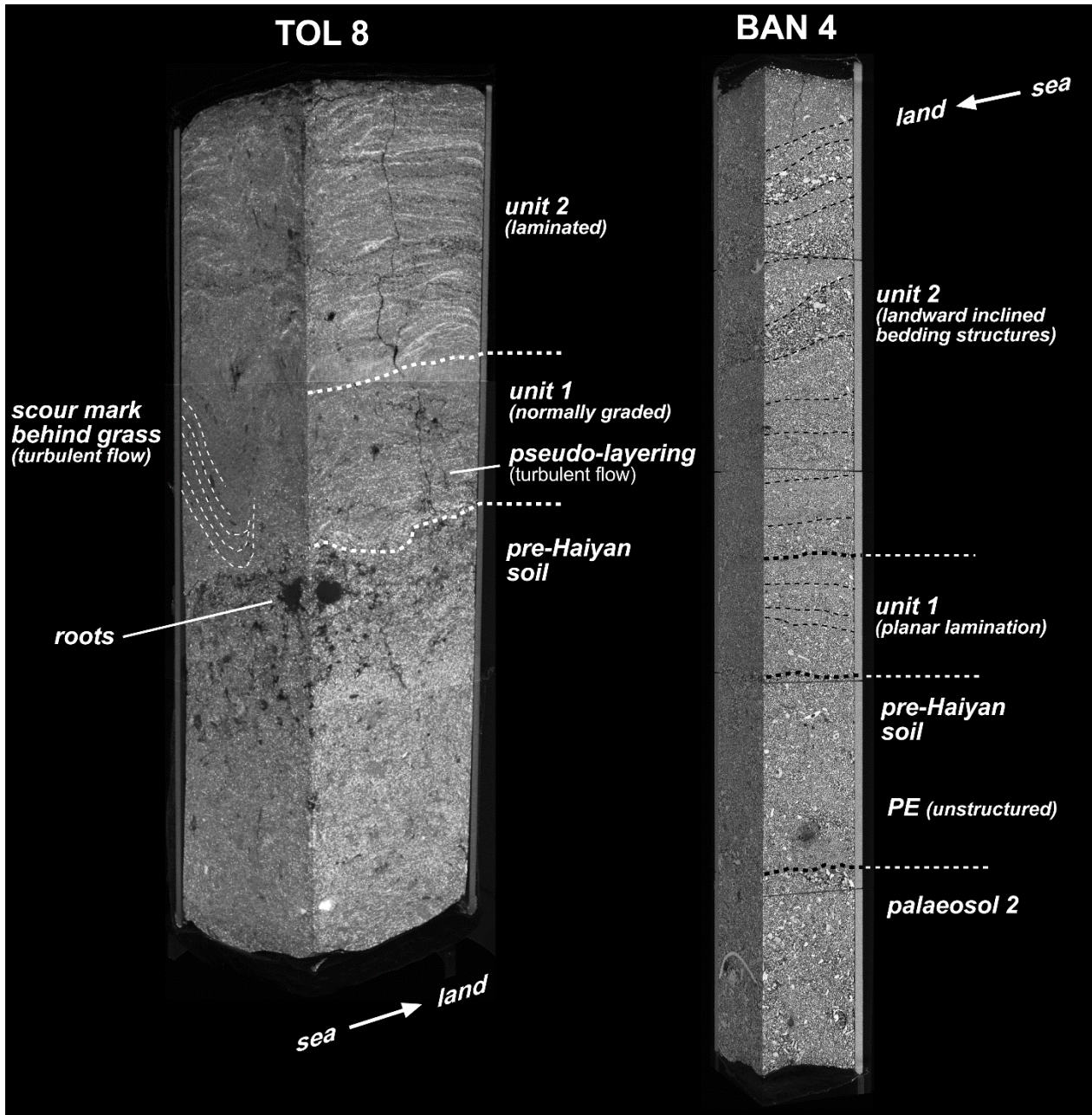
Fig. 7: µCT scans of sediment cores TOL 8 and BAN 4 (as for locations see figures 5d and 10f, respectively). The 3D data support the documentation and interpretation of sedimentological features and different units within the typhoon deposits. The basal unit of TOL 8 is slightly normally graded and characterized by scour structures behind bended grass stems (unit 1). The upper part is horizontally laminated (unit 2). In BAN 4 the deposit of Typhoon Haiyan clearly contrasts the unstructured pre-Haiyan sediments composed of two palaeosols separated by an older sand sheet. It is divided into a planar bedded unit 1 at the base, and steeply landward inclined laminae in unit 2.
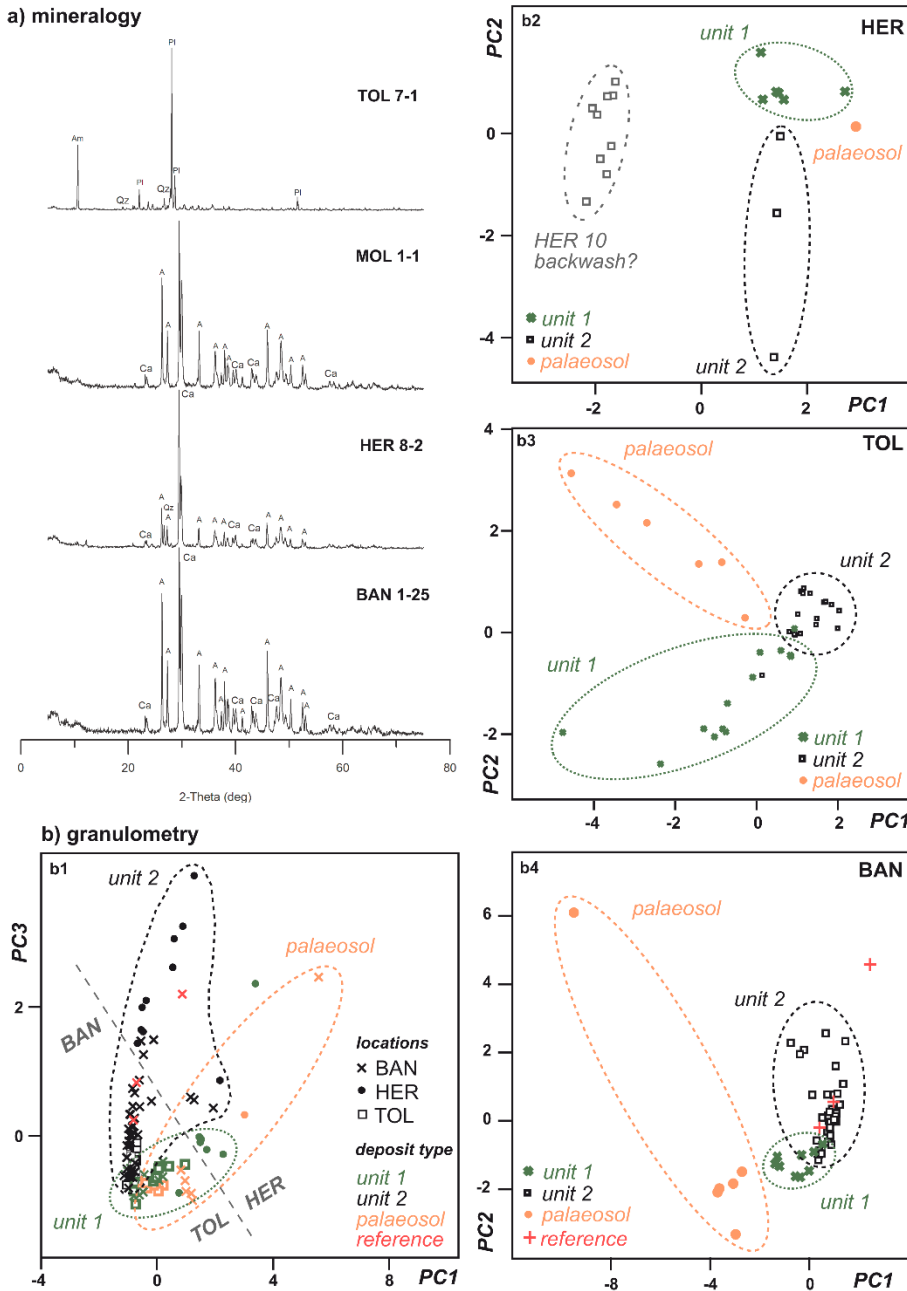
Fig. 8: PCA results for sandy deposits of Typhoon Haiyan. a) XRD studies allow for a separation of deposits from carbonate coasts (MOL, HER, BAN) and the siliclastic coast (TOL) on the basis of bulk-mineralogy. Ca = calcite, A = aragonite, Qz = quartz, Pl = plagioclase, Am = amphibole. b) Grain-size data reflect both site-specific characteristics (TOL, BAN, HER) and differences in formation (unit 1, unit 2, palaeosol) (b1). A discrimination of sediment formation (unit 1, unit 2, palaeosol) due to particular clusters is even more pronounced on the intra-site level (b2-4).
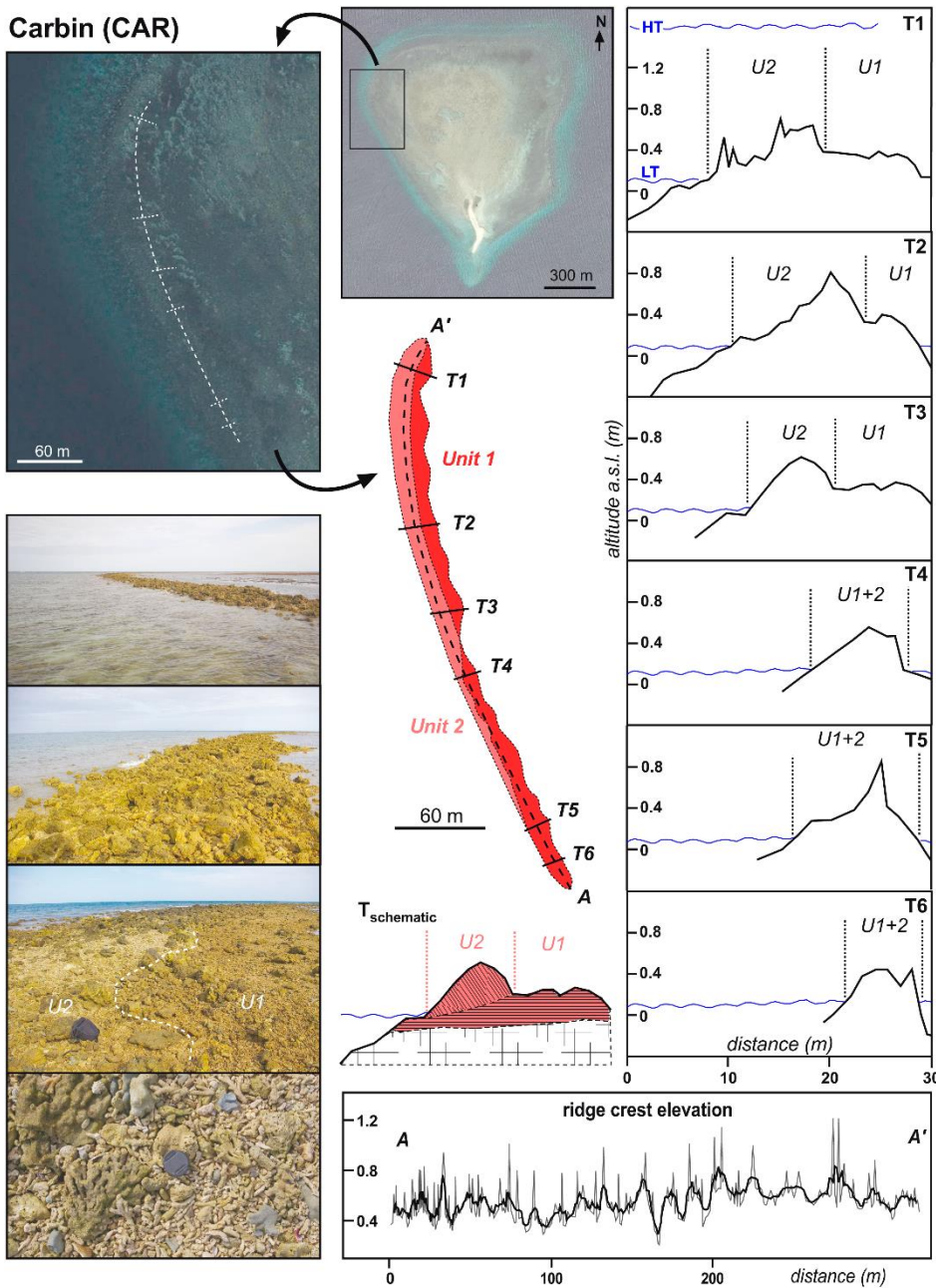
Fig. 9: Carbin Reef (CAR) study site with typhoon-generated coral rubble ridge. The ridge at the western edge of the reef platform shows no clear trend of crest elevation, but significant differences in width and shape between six coast-perpendicular transects (T1–T6). In the northern part of the ridge, flat and up to 30 m wide lobes composed of algae-covered, greyish coral fragments form the basal unit of the ridge (U1). Unit 1 is topped by steeper lobes with a significant percentage of freshly broken coral fragments that occur along the whole ridge section but reach widths of only 10 m (U2). The presence of two morpho-stratigraphical units might be due to either changing wind directions during formation entirely by Haiyan, or due to the impact of successive storms where Haiyan only deposited the uppermost unit.
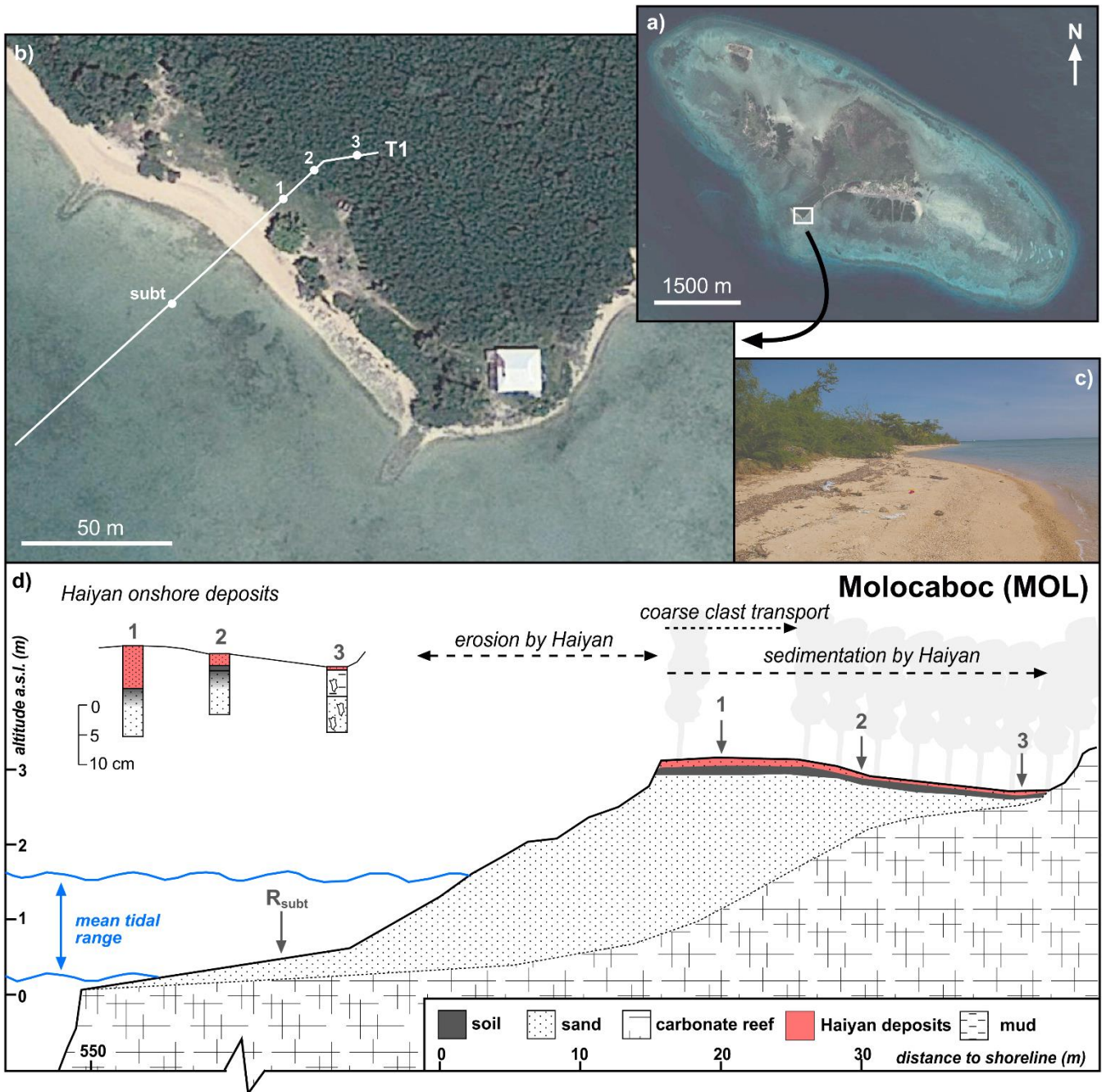
Fig. 10: Molocaboc study site (MOL) with depositional and geomorphological effects of Typhoon Haiyan. a) Location of studied beach section on Molocaboc. b) Onshore sediments of Haiyan were investigated in three trenches (MOL 1–3) along a shore-perpendicular transect (T1). c) Beach profile after the Haiyan impact (view towards SE; date: 20 Feb 2014). d) Topographical cross section: the pre-Haiyan beach was substantially eroded and Haiyan generated a landward thinning sand sheet reaching up to 40 m inland in the back-barrier depression.

Fig. 11: Bantayan study sites (BAN A and BAN B) with documented flood marks and geomorphological impact of Typhoon Haiyan.
a–b) At BAN A, Haiyan flooded the proximal part of the back-barrier plain and formed a series of overlapping, small washover fans
directly behind the beach ridge (based on Google Earth/Digital Globe 11/11/2013 [inset in b: 04/27/2001]). c) The washover fans
5 **reveal flat lobes at the base (U1), and steep lobes on top (U2). d–e) At BAN B, flooding levels of more than 3 m a.s.l. generated several**
distinct washover fans (based on Google Earth/Digital Globe 11/11/2013).
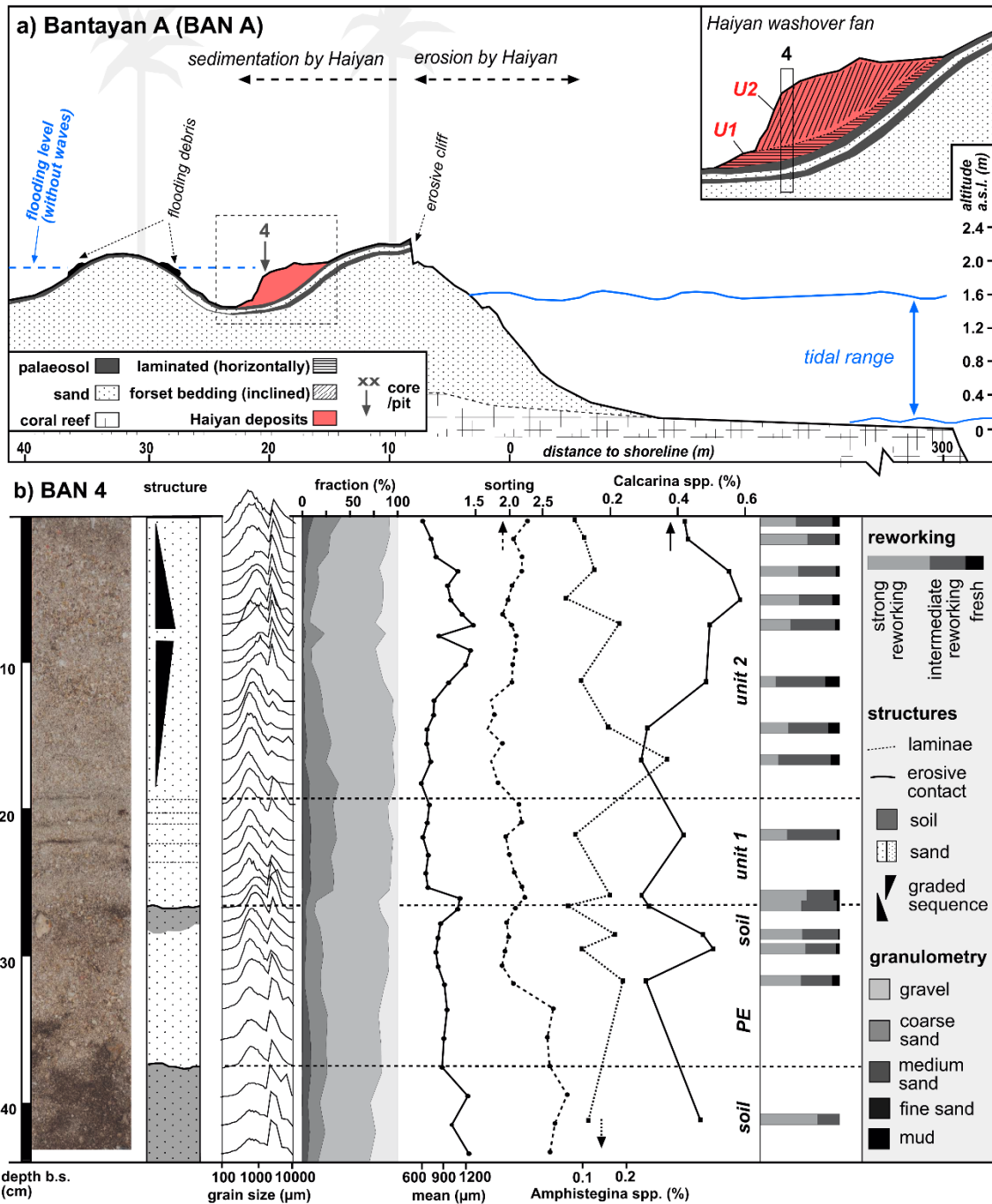
Fig. 12: Typhoon Haiyan onshore deposits at site BAN A. a) A shore-perpendicular cross section (see Fig. 11 for location) reveals two sedimentary units within the washover fans, a flat and planar laminated unit at the base (U1), and steep, landward inclined lobes on top (U2). Below the pre-Haiyan soil, a second palaeosol is covered by a thin sand layer (PE), possibly a former extreme wave event. **b)** Sedimentary characteristics of core BAN 4. The 26 cm thick Haiyan deposits are clearly separated from older sediments by an initial soil formation. While the basal unit 1 is laminated, unit 2 is characterised by gradual coarsening, changing foraminifer composition (more *Calcarina* spp., less *Amphistegina* spp.) and a decreasing percentage of fresh foraminifer tests towards the top.
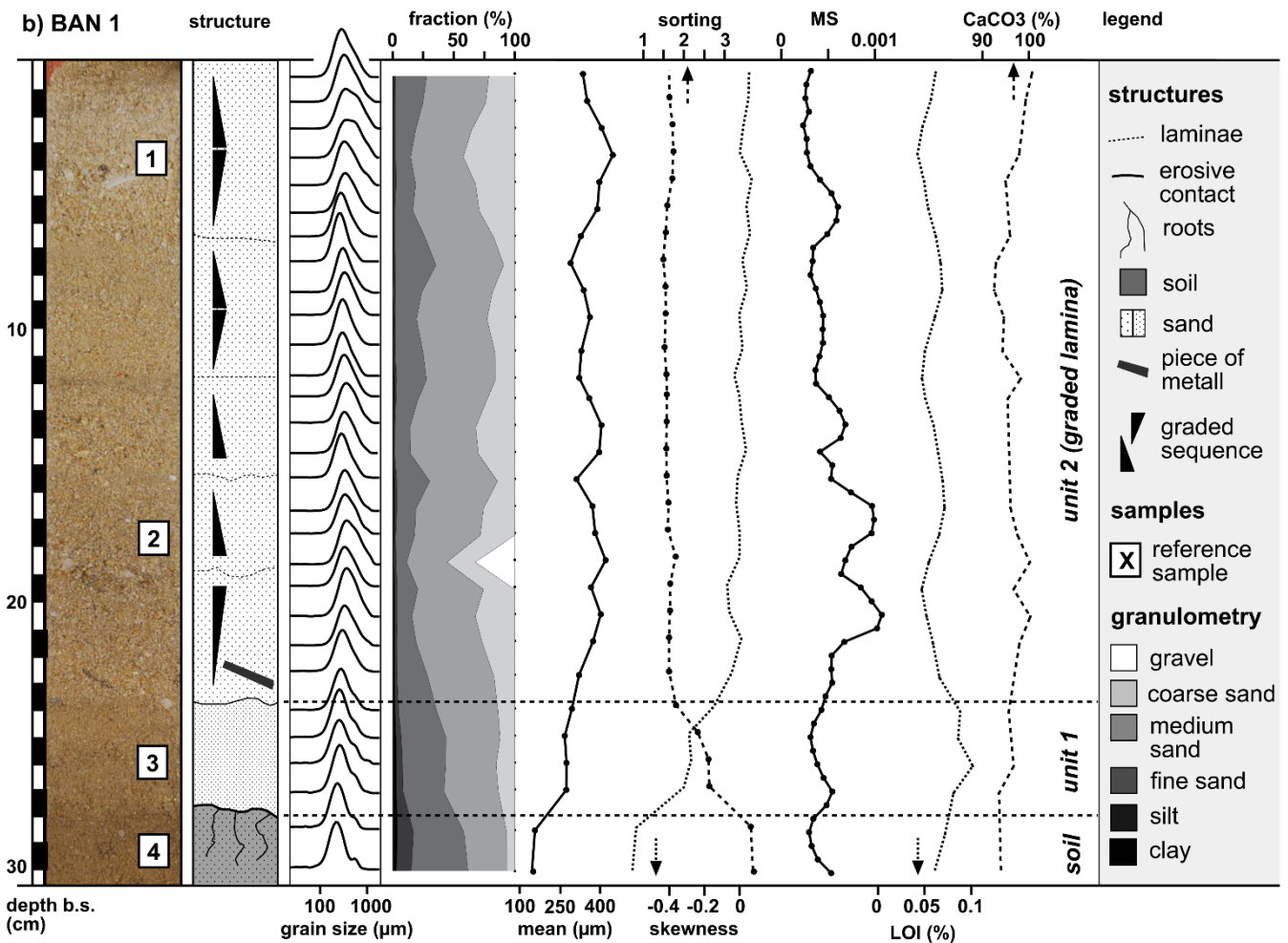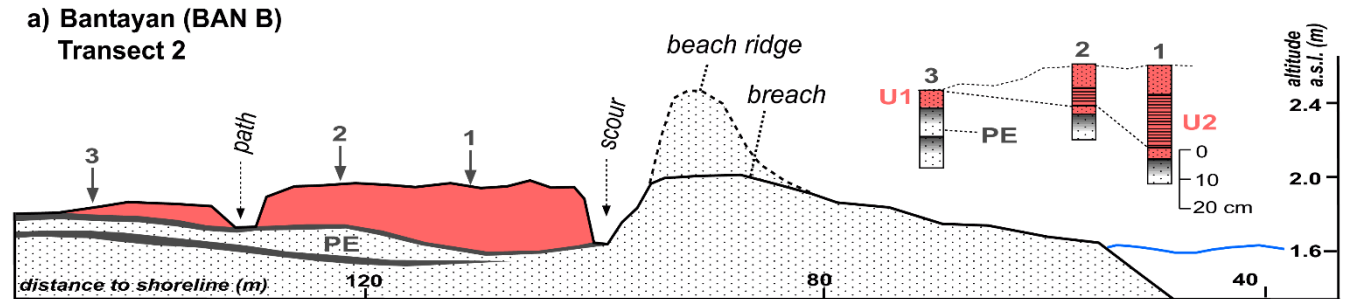
Fig. 13: Sedimentary characteristics of Typhoon Haiyan deposits at site BAN B. a) Transect 2 (see Fig. 11 for location) reveals a landward thinning structure directly behind a storm-induced breach in the coastal barrier. A massive sand sheet at the base (U1) is overlain by a laminated section (U2) in the proximal part of the washover fan. b) BAN 1 is composed of two distinct units, a massive unit at the base (unit 1) and a laminated unit on top (unit 2).